Marine Geophysical Researches **21:** 423–450, 2000.

Recent tectonics of the Blanco Ridge, eastern blanco transform fault zone

Robert P. Dziak[1], Christopher G. Fox[2], Robert W. Embley[2], John L. Nabelek[3], Jochen Braunmiller[3] & Randolph A. Koski[4]

[1]*Cooperative Institute for Marine Resources Studies, Oregon State University, Hatfield Marine Science Center, Newport, OR 97365, USA* [2]*National Oceanic and Atmospheric Administration, Pacific Marine Environmental Laboratory, Hatfield Marine Science Center, Newport, OR 97365, USA* [3]*College of Ocean and Atmospheric Sciences, Oregon State University, Corvallis, OR 97331, USA* [4]*United States Geological Survey, MS999 345 Middlefield Rd, Menlo Park, CA 94025, USA*

Received 25 August 1998; accepted 23 May 2000

Key words: Blanco transform fault zone, earthquakes, ridge formation, submersible

Abstract

Bathymetric, hydro-acoustic, seismic, submersible, and gravity data are used to investigate the active tectonics of the eastern Blanco Transform Fault Zone (BTFZ). The eastern BTFZ is dominated by the ∼150 km long transform-parallel Blanco Ridge (BR) which is a right-lateral strike-slip fault bordered to the east and west by the Gorda and Cascadia Depressions. Acoustic locations, fault-parameter information, and slip vector estimates of 43 earthquakes ($M_w \geq 3.8$) that occurred along the eastern BTFZ over the last 5 years reveal that the Blanco Ridge is a high-angle right-lateral strike-slip fault, with a small component of dip-slip motion, where the Juan de Fuca plate is the hanging wall relative to the Pacific plate. Furthermore, the Cascadia and Gorda basins are undergoing normal faulting with extension predominantly oblique to the transform trend. Seafloor submersible observations agree with previous hypotheses that the active transform fault trace is the elongate basin that runs the length of the BR summit. Brecciated and undeformed basalt, diabase, and gabbro samples were collected at the four submersible survey sites along the Blanco Ridge. These petrologic samples indicate the Blanco Ridge is composed of an ocean crustal sequence that has been uplifted and highly fractured. The petrologic samples also appear to show an increase in elevation of the crustal section from east to west along the Blanco Ridge, with gabbros exposed at a shallower depth farther west along the southern (Pacific plate side) BR ridge flank. Further supporting evidence for BR uplift exists in the seismic reflection profiles across the BR showing uplift of turbidite sequences along the north and south ridge base, and gravity and magnetics profiles that indicate possible basement uplift and a low-density zone centered on the ridge's Pacific plate side. The BR formation mechanism preferred here is first, uplift achieved partially through strike-slip motion (with a small dip-slip component). Second, seawater penetration along the fault into the lower crust upper mantle, which then enhanced formation and intrusion of a mantle-derived serpentinized-peridotite diapir into the shallow ocean crust, causing further uplift along the fault.

Introduction

The Blanco Transform Fault Zone (BTFZ), located in the northeast Pacific Ocean off the coast of Oregon, is a 350 km long right-lateral strike-slip transform fault that links the moderate-spreading rate Juan de Fuca and Gorda Ridges (Figure 1). Utilizing available high resolution bathymetry, Embley and Wilson (1992) divided the BTFZ into five major right-stepping strike-slip fault segments that are separated by deep extensional basins. The majority of these basins were interpreted to be the oceanic analog of pull-apart basins observed along continental divergent wrench fault systems, while one, the Cascadia Depression, was interpreted as a proto-spreading center (deCharon, 1988). The BTFZ has long been known to generate large earthquakes ($m_b > 6$) that are tectonic in origin (Tobin and Sykes, 1969; Chandra, 1974; Dziak et al., 1991). The Blanco Ridge (BR), the fault segment that connects the Cascadia and Gorda Depressions, is the longest structurally uninterrupted strike-slip fault segment within the BTFZ (∼150 km in length). Accordingly, the largest earthquakes within the entire BTFZ have occurred along the BR, with five earthquakes of $m_b \geq 6$ occurring in the last 30 yr (Dziak et al., 1991). However, comparison of BTFZ slip rates

estimated from plate motion models to slip rates estimated from seismic moment release over the past 30 yr suggests that >80% of the slip along the BTFZ is occurring aseismically (Dziak et al., 1991). This may be due to the thermal character of oceanic crust along transform faults, with elevated crustal isotherms that may result in a less well coupled fault zone (Bergman and Solomon, 1988).

The Blanco Ridge is an example of one of the more enigmatic features observed along fracture zones throughout the world, the transform-parallel or transverse ridge. Origins proposed for these transform ridges range from serpentinite intrusion (Bonatti, 1976; Bonatti, 1978) to volcanism resulting from extension across the transform (Thompson and Melson, 1972), to dip-slip faulting from a component of extension or compression (Bonatti, 1978). Models of a Blanco Ridge formation mechanism have generally been hampered by a lack of data, since prior to this work rock samples have been recovered from only two sites along the BR's extreme east and west ends. During August and September of 1994, a dive program utilizing the U.S. Navy's DSV *Turtle* and Advanced Tethered Vehicle (ATV) was carried out along the Blanco Ridge and Gorda Depression to map significant structural features and better understand eastern BTFZ tectonics and BR formation.

The availability of the U.S. Navy's SOund SUreveillance System (SOSUS) hydrophone arrays to the scientific research community in combination with the recent establishment of a broadband seismograph network allows for monitoring of the Juan de Fuca plate seismicity with unprecedented location accuracy and source parameter detail. The purpose of this study is to combine the preliminary geologic mapping and petrologic results of the 1994 BTFZ dive series with the recent earthquake moment-tensor solutions, SOSUS earthquake locations, and recently-collected high resolution bathymetry to understand better the state of stress and the mechanics of crustal deformation along the eastern BTFZ. Based on analysis of this new data, a preferred model of the formation mechanism for the Blanco Ridge is proposed.

The formation mechanism for transform ridges is an important question for many fields of study. Earthquakes associated with the deformation and uplift of transform ridges can be quite large and therefore may be a seismic and tsunami hazard to nearby coastal communities. The uplift of transform ridges has the potential to effect the circulation pattern of oceanic currents and therefore regional climates (Fisk et al., 1993). The obduction of transform ridges may be one mechanism by which ophiolites are preserved in continental settings.

Blanco ridge tectonic setting and regional morphology

The Blanco Ridge (BR) occurs along the right-lateral strike-slip fault segment, trending at about 111°, that forms the eastern portion of the Blanco Transform Fault Zone connecting the pull-apart basins of the Cascadia and Gorda Depressions. Figure 1 shows the Blanco Ridge bathymetry with the location of faults, fracture zones, and turbidite channels identified from the bathymetry, while Figures 2 and 3 show three-dimensional perspectives of the ridge. The Blanco Ridge is composed of a series of lozenge-shaped highs with about 600 to 1000 m of bathymetric relief, and varying from 3.5 km wide just north of the Gorda Depression to 7 km wide about midway between the Gorda and Cascadia Depressions. The shoalest point along the Blanco Ridge is at 128°00′ W, where the ridge rises to less than 1900 m deep. West of its shoalest point, the ridge deepens until it ends at the intersection with the SE corner of the Cascadia Depression at 128°40′ W. From 128°35′ W to 128°20′ W, a series of back-tilted normal fault blocks from the Cascadia Depression form the northwestern boundary of the Blanco Ridge. The blocks direct the Cascadia Channel along the base of the Blanco Ridge and into the Cascadia Depression. South of the ridge, between 127°50′ W and 127°35′ W, the Pacific plate exhibits a series of bent abyssal ridges.

The detailed bathymetry of the ridge from about 128°00′ W to 127°40′ W reveals a series of closed basins and lineaments which collectively appear to follow the 111° BTFZ trend, at least along distances of about 10 km. These features were interpreted by Embley and Wilson (1992) to delineate the zone of most recent strike-slip faulting. Indeed, these narrow basins can be traced as a long narrow lineation along the summit of the Blanco Ridge (identified by black arrows in Figures 2 and 3), and could be the active transform fault zone. The narrow cross-section of the Blanco Ridge and the lack of any obvious volcanic-constructional features (such as small cones) make a volcanic origin of the ridge highly unlikely. Ibach (1981) presents a seismic reflection profile across the north side of the ridge between 127°30′ W and 128°05′ W that shows an uplifted bench of a layered

turbidite sequence (Figure 2, identified by the white arrows). This bench shows ∼300 m of uplift from east to west along the north side of the Blanco Ridge. Along the north flank of the turbidite bench, there is a pronounced lineation (L1 in Figure 1; shown by the white arrows in Figure 2) not identified by either Ibach (1981) or Embley and Wilson (1992). The trend of L1 is oblique to the Sea Beam tracklines, suggesting that this lineament is a real feature in the seafloor and not an artifact of non-overlapping swaths as illustrated by the linear data gap just above the upper white arrow in Figure 2. There is also a similar lineament along the south side, and parallel to, the Blanco Ridge between 127°40′ W and 127°20′ W (L2 in Figure 1; white arrows, Figure 3).

North of the Blanco Ridge, between 128°05′ W and 127°12′ W, the Cascadia Deep-Sea Channel (dotted line, Figure 1) parallels the Blanco Ridge and cuts into flat-lying turbidites (Ibach, 1981; Embley, 1985), before turning southwest to flow between the Cascadia Depression back-tilted fault blocks (deCharon, 1988) and the BR (dotted line in Figure 1). Embley (1985) has described a secondary channel system (identified by the southward pointing v-shaped drainage pattern north of the BR) that drains in to the Cascadia Channel. Erosion of these channels may result from slumps and turbidity currents from the sediment bench on the ridge's north side, and as a result of backcutting from deepening of the Cascadia Channel base level.

The Blanco Ridge is bounded to the east and west by two pull-apart basins, the Gorda and Cascadia Depressions, respectively (Embley and Wilson, 1992). The Cascadia Depression (CD) is bounded on either side by a series of inward-facing back-tilted blocks which are covered by a thick turbidite sequence (Griggs and Kulm, 1973). The CD normal faults are oriented about 10° to 15° from orthogonal to strike of the southern (BR) and northern bounding transform faults. The CD normal faults and back-tilted blocks also appear to be rotated counterclockwise relative to the BR and the observed structure just to the north in the Juan de Fuca plate. The Cascadia Channel thalweg drops 130 m as it enters the CD, which was interpreted by Griggs and Kulm (1973) to be a result of CD subsidence at a rate of 1.8 cm yr^{-1} over the last 6.6 ka. Seismic reflection profiles suggest there is up to 500 m of sediment in the CD, with a small 60 m relief ridge in the center of the basin flanked by small (5–10 m relief) back-tilted fault blocks that mirror the large-scale structures surrounding the basin (deCharon, 1988). Also, acoustic opaque zones in the seismic reflection profiles have been cited as evidence for igneous intrusion within the basin fill (Embley et al., 1987). The point at which the active strike-slip fault from the BR enters the CD seems to be represented as a small linear trough along the southern edge of the Cascadia Channel (Figure 2).

To the east, the Blanco Ridge merges with the northern edge of the Gorda Depression (GD). Here too the active fault trace, as it enters the northwestern edge of the basin (Figure 3), seems to be delineated by a linear trough along the north and south sides of the depression. Based on its rhomb-graben morphology, Embley and Wilson (1992) concluded that the GD was formed by extension between two strike-slip fault strands; the BR to the north and a strike-slip fault strand along its southern border extending to the Gorda Ridge. Sea Marc II side scan data suggests the presence of lava flows emanating from fissures on the floor of the GD (Clague and Holmes, 1987), however dredge samples across the basin provided no fresh basalts. Fault blocks identified from bathymetry within the Gorda Depression appear to be rotated even more counter-clockwise (∼20°–25°) to the trend of the BR than those within the Cascadia Depression. The GD is bounded by longer strike-slip fault segments than is the CD, which suggests the GD comprises a more diffuse zone of oblique faulting. As a result, the GD fault blocks may undergo a significant component of strike-slip motion, and are thus not labeled as only normal faults. Also noteworthy is that the Blanco Ridge is not present along the north side of the GD between 126°50′ W and 126°45′ W (red arrow, Figure 3). Along that section of the ridge, there is a large (∼2–3 km) arcuate basin (tip of red arrow), which looks very similar to a slump scar. Thus we interpret that the Blanco Ridge may be missing here because the ridge was unstable (perhaps from overburden pressure, or even seismic shaking) and slumped into the GD. There is not, however, a clear debris flow at the base of the slump scar. This may be due to the material being rapidly deformed by the tectonically active GD, or if the slump is relatively old, perhaps the debris flow was rafted well westward by transform motion.

Magnetic anomaly data indicate the Cascadia Depression and Blanco Ridge strike-slip fault formed as a result of a clockwise change in Juan de Fuca - Pacific plate motion at about 5 Ma (Wilson et al., 1984; Wilson, 1993). The Cascadia Depression may be a remnant of a rift segment that died as a result of a southward propagation event about 5 Ma (Embley and

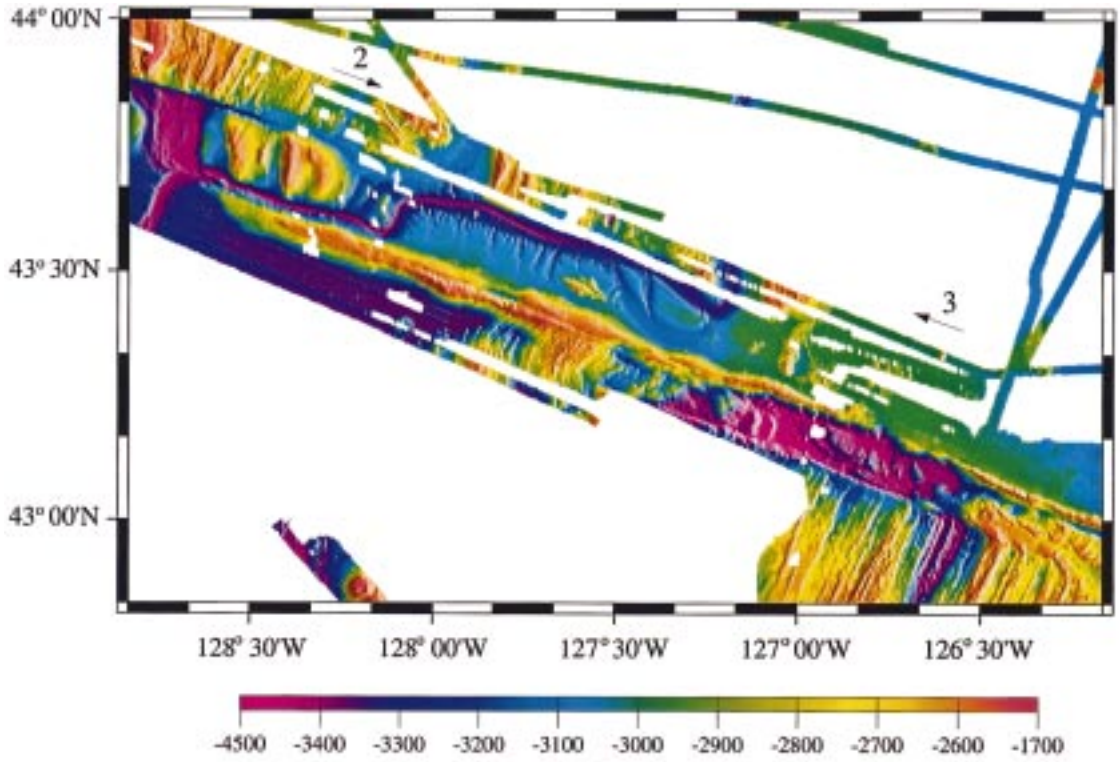
44° 00'N
43° 30'N
43° 00'N
128° 30'W
128° 00'W
127° 30'W
127° 00'W
126° 30'W
2
3
-4500
-3400
-3300
-3200
-3100
-3000
-2900
-2800
-2700
-2600
-1700

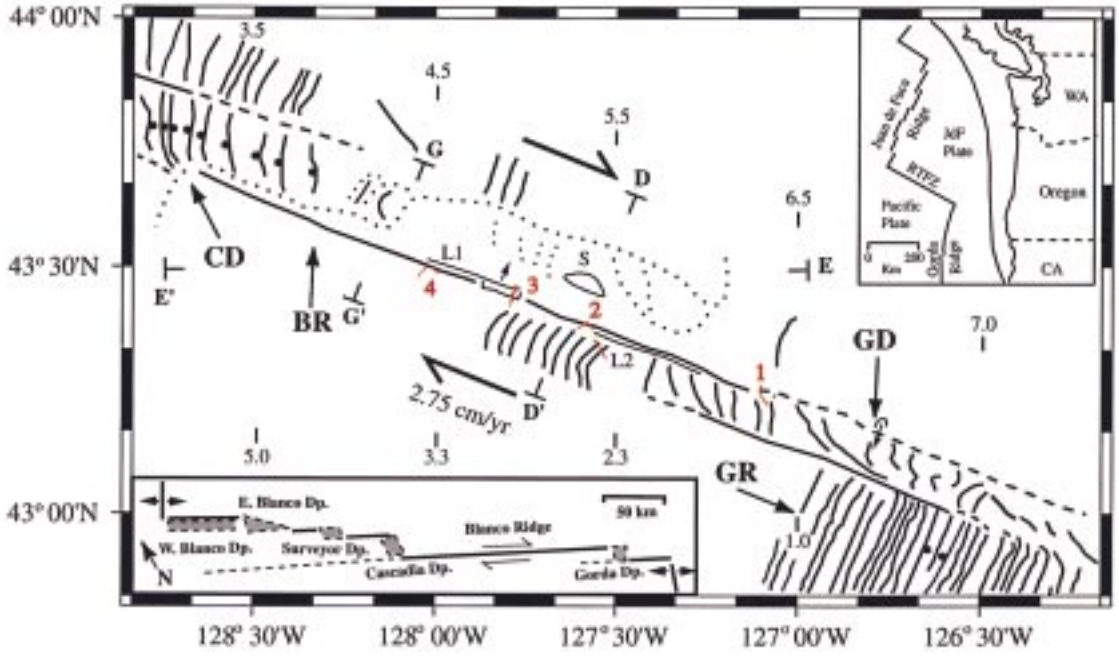
44° 00'N
43° 30'N
43° 00'N
128° 30'W
128° 00'W
127° 30'W
127° 00'W
126° 30'W
3.5
4.5
5.5
6.5
7.0
5.0
3.3
2.3
1.0
G
D
E
E'
CD
BR
G'
L1
L2
S
1
2
3
4
2.75 cm/yr
D'
GD
GR
E. Blanco Dp.
W. Blanco Dp.
Surveyor Dp.
Blanco Ridge
Cascadia Dp.
Gorda Dp.
50 km
N
Juan de Fuca Ridge
JdF Plate
RTFZ
Pacific Plate
Gorda Ridge
WA
Oregon
CA
0
180
Km

Figure 1. (Top) Sea Beam bathymetric map of the Cascadia Depression, Blanco Ridge, and Gorda Depression, eastern Blanco Transform Fault Zone (BTFZ). Multibeam bathymetry was collected by the NOAA R/V's *Surveyor* and *Discoverer* and the R/V *Laney Chouest* during 12 cruises in the 1980's and 90's. Bathymetry displayed using a 500 m grid interval. Numbers with arrows show look directions of three-dimensional diagrams in Figures 2 and 3. (Bottom) Structure map, interpreted from bathymetry, showing active faults and major geologic features of the region. Solid lines represent faults, dashed lines are fracture zones, and dotted lines show course of turbidite channels. When possible to estimate sense of motion on a fault, a filled circle shows the down-thrown side. Inset maps show location and generalized geologic structure of the BTFZ. Location of seismic reflection and gravity/magnetics profiles indicated by opposing brackets. D-D' and E-E' are the seismic reflection profiles shown in Figures 8a and 8b, and G-G' is the gravity and magnetics profile shown in Figure 13. Submersible dive tracklines from sites 1 through 4 are highlighted in red. L1 and L2 are two lineations seen in three-dimensional bathymetry shown in Figures 2 and 3. Location of two Blanco Ridge slump scars indicated by half-rectangles, inferred direction of slump shown by arrow, and debris location (when identified) designated by an 'S'. CD stands for Cascadia Depression, BR is Blanco Ridge, GD is Gorda Depression, and GR is Gorda Ridge. Numbers on north and south side of transform represent Juan de Fuca and Pacific plate crustal ages inferred from magnetic anomalies. Long-term plate motion rate between the Pacific and southern Juan de Fuca plates from Wilson (1989).

Wilson, 1992). The Gorda Depression may have originated in a similar way about 1–2 Ma. Embley and Wilson (1992) speculate that a component of extension or compression across the BTFZ is resisting the development of a single through-going transform fault. Ibach (1981) proposed that there is compression across the Blanco Ridge as evidenced by the uplifted turbidite bench. Since the best seismological evidence at that time indicated the Blanco Ridge was undergoing pure strike-slip faulting (Chandra, 1974), Embley and Wilson (1992) suggested the bench uplift was a result of serpentinite diapirism. Further, they suggested that between extension and compression along the Blanco Ridge, extension seemed more likely. The obliquity in the strikes of the BR and Mendocino Transform would tend to produce compression across the Mendocino, and extension across the Blanco Ridge.

Figure 1 shows the approximate ages of the Juan de Fuca and Pacific plates, estimated from magnetic anomalies by Wilson (1993), along adjoining sections of the transform. Crust of the Pacific plate is considerably younger (2.75–7.0 Ma) than that of the Juan de Fuca plate from the Gorda Ridge west to 127°30′W. West of 127°30′W the two plates are similar in age, with the Juan de Fuca plate ∼1.5 Ma younger than the Pacific near the Cascadia Depression. This relative age difference could affect the relative buoyancy of the two plates and hence the style of faulting along the transform. The older plate may tend to subside relative to the younger plate during strike-slip faulting, resulting in a component of dip-slip motion during a given earthquake. It is interesting to note that the pull-apart basins are located where the relative age differences between the Juan de Fuca and Pacific plates becomes significantly > 2 my, suggesting the subsidence of the older plate plays a role in the stability and development of these pull-apart basins.

T-wave locations, focal mechanisms, and slip vector information

The U.S. Navy's SOSUS hydrophone data were analyzed by the National Oceanic and Atmospheric Administration's Pacific Marine Environmental Laboratory. Offshore earthquakes are detected and located from the acoustic data utilizing the event's water-borne Tertiary (T-) wave. Precisely known ocean sound speed models and an array geometry that is much improved over land-based seismic networks allows for highly accurate (±3 km error in latitude and longitude) event locations over a wide range ($2.0 \leq M \leq 7$) of magnitudes (Fox et al., 1994). Seismograph-derived epicenters for NE Pacific ocean earthquakes typically have a 10 to 35 km northeastward bias in location (Dziak et al., 1991). Although the hydrophone array locations are not for public distribution, the hydroacoustic earthquake locations are not classified. Effective, routine estimation of oceanic earthquake source moment tensors, depths, and source time functions for events of magnitude 4.0 and larger has been demonstrated using the Pacific-Northwest broadband array (Nabelek and Xia, 1995; Braunmiller et al., 1995). The broadband array, deployed in 1992, consists of over twenty digital 3-component broadband high-dynamic range seismic stations distributed along coastal northern California, Oregon, Washington, and British Columbia (Nabelek and Xia, 1995).

Figures 4 and 5 show bathymetry, earthquake focal mechanisms, and epicenters of 43 earthquakes ($3.8 \leq M \leq 6.5$) that occurred along the Blanco Ridge between August, 1992 to February, 1997. The earthquakes were located by the NOAA T-phase Project using acoustic earthquake data recorded by the SOSUS hydrophone arrays. The SOSUS locations, location error, and magnitudes, and seismic locations, magnitudes, and Centroid Moment Tensor information are summarized in Tables 1 and 2. In Table 1, the seis-

Table I. Earthquake origin times, locations, and magnitudes

Event	Date	OT	Seismic		h (km)	MAG	OT	SOSUS		Mag (dB)
			Lat (°)	Lon (°)				Lat (°)	Lo, (°)	
1	080492	142741.2	43.468	−127.014	015	b4.9	142713	43.185	−127.074	229.1
2	082192	010218.4	43.930	−128.344	015	b5.5	010202	43.791	−128.682	227.5
3	111792	203720.0	44.096	−128.543	006	w4.8	203646	43.772	−128.674	228.2
4	050993	221649.0	43.717	−128.120	006	w5.0	221604	43.450	−128.003	228.4
5	011994	011626.0	43.630	−128.150	009	w5.7	011600	43.328	−127.450	230.6
6	061494	020415.0	43.825	−128.293	006	w4.9	020351	43.580	−128.237	228.7
7	063094	073045.0	43.745	−127.984	006	b4.3	073015	43.537	−128.314	223.2
8	071394	175246.0	43.450	−126.648	006	w5.2	175217	43.085	−126.786	224.9
9	072294	224415.0	43.320	−126.846	006	w4.4	224355	43.121	−127.040	225.5
10	081294	112619.0	43.877	−126.397	009	w4.1	112506	43.832	−128.695	222.7
11	102794	043827.0	43.216	−126.698	004	w4.7	043840	43.025	−126.248	228.6
12	102794	174556.0	43.630	−127.340	015	w6.5	174511	43.595	−128.219	226.3
13	103094	022325.0	43.448	−127.417	009	w4.9	022313	43.306	−127.234	225.4
14	103094	205414.0	43.647	−127.194	006	w4.4	205356	43.486	−128.072	224.3
15	110294	204836.0	43.799	−127.854	004	w5.1	204815	43.550	−128.018	227.5
16	110694	040442.0	43.675	−127.464	006	w4.9	040430	43.288	−127.174	225.2
17	110794	150251.0	43.557	−127.107	009	w4.6	150235	43.294	−127.143	226.6
18	112294	212322.0	43.483	−127.687	006	w5.0	212310	43.406	−127.553	228.1
19	032895	034345.0	43.372	−127.053	006	w4.0	034333	43.233	−127.077	223.5
20	050495	061852.0	43.189	−126.687	006	w4.2	061850	43.022	−126.701	211.8
21	051295	235046.0	43.389	−127.255	006	w4.1	235036	43.392	−127.442	226.1
22	051395	060349.0	43.534	−127.171	006	w4.7	060336	43.389	−127.442	229.9
23	080395	054159.0	43.177	−126.709	006	w4.2	054137	43.160	−126.782	223.6
24	090295	094135.0	43.764	−128.499	009	w4.6	094145	43.812	−128.693	218.3
25	092595	075824.0	43.752	−128.515	009	w5.0	075808	43.812	−128.746	222.5
26	092595	080149.0	43.752	−128.515	009	w4.5	080126	43.840	−128.709	212.7
27	092695	013915.0	43.319	−127.160	006	w5.4	013833	43.151	−127.061	222.7
28	101595	064952.0	43.668	−128.540	006	w3.8	064949	43.603	−128.491	217.6
29	101995	145957.0	43.312	−127.277	010	w4.3	150058	43.292	−127.257	221.4
30	122495	025122.0	43.270	−127.043	004	w4.6	025058	43.163	−127.053	223.7
31	020696	053200.0	43.689	−128.369	004	w4.2	053152	43.598	−128.388	226.7
32	022096	005210.0	43.212	−127.144	004	w5.3	005147	43.143	−126.907	228.8
33	022096	012111.0	43.218	−127.162	006	w4.4	012105	43.275	−127.107	227.6
34	041596	122924.0	43.474	−127.711	004	w5.4	122917	43.434	−127.717	230.1
35	051896	191401.0	43.390	−127.633	004	w4.5	191352	43.336	−127.434	227.1
36	071796	223615.0	43.143	−127.182	006	w4.2	223611	43.161	−127.054	221.2
37	101696				006	w4.4	125033	43.344	−127.596	222.1
38	101696				009	w4.2	130740	43.337	−127.580	218.1
39	110496				006	w5.5	225405	43.337	−127.479	228.7
40	111996				004	w4.5	221959	43.139	−126.912	222.2
41	112496				006	w4.4	182228	43.179	−126.969	224.1
42	011397	163252.0	43.537	−128.181	004	w4.5	163250	43.561	−128.232	225.4
43	022097				006	w4.5	110.44	43.287	−127.398	227.2

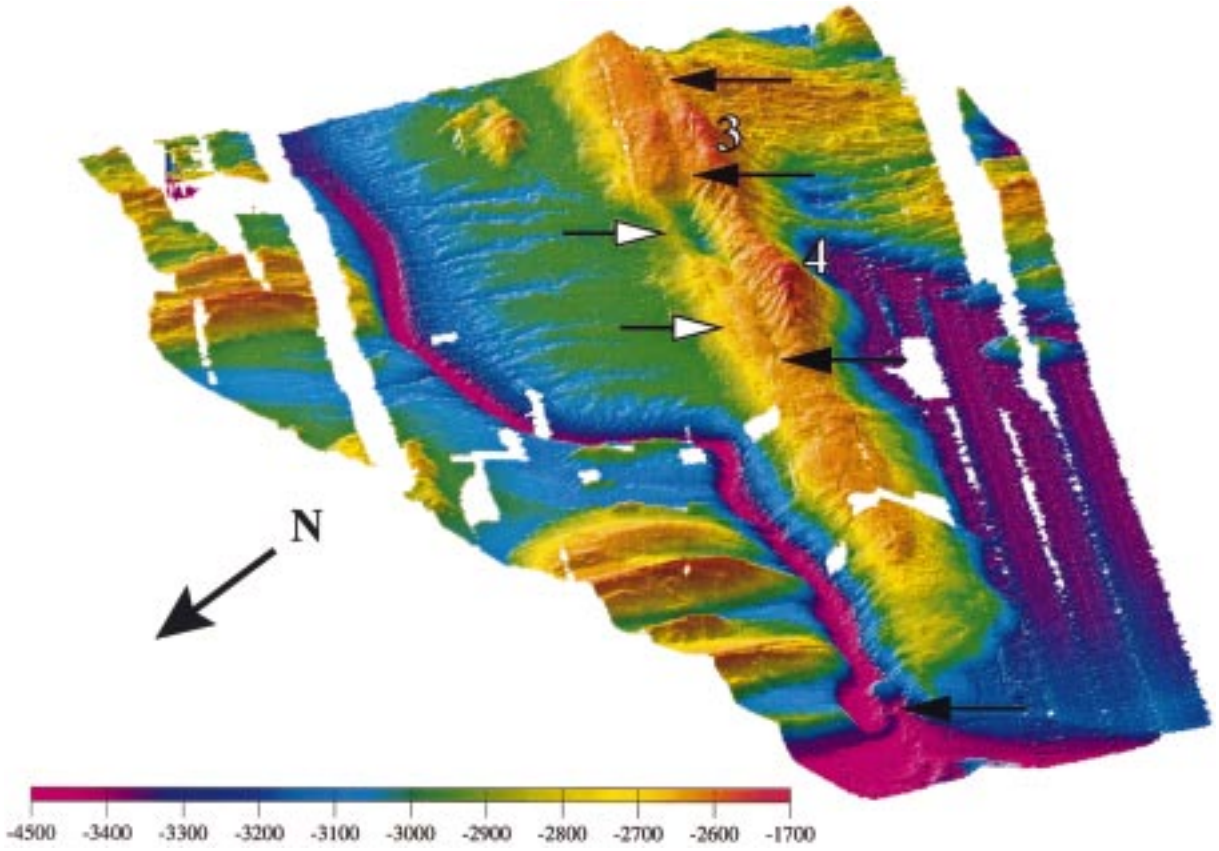

Figure 2. Three-dimensional perspective of bathymetry from the western half of the Blanco Ridge and Cascadia Depression. Bathymetry displayed using a 200 m grid interval. Black arrows delineate transform-parallel linear notch at the BR summit, which is the probable active transform fault trace. White arrows highlight uplifted turbidite bench identified by Ibach (1981), and a lineation (L1 in Figure 1) that cuts the bench. The lineation may be fault generated, and not simply an error due to bathymetric swath offsets. The numbers show the location of dive sites 3 and 4.

mic magnitude is either body-wave (b) or moment (w) magnitude, the SOSUS heading represents the acoustically derived location for each event, and the acoustic magnitude is in decibels (dB). Acoustic magnitudes were calculated by converting the maximum amplitude of the T-wave signal packet from voltage to units of power, then finding the average magnitude of all hydrophones that recorded earthquake. The earthquake locations were estimated by hand-selecting T-wave arrival times recorded on ($\geq$ 3) individual hydrophones from throughout the northeast Pacific Ocean. Earthquake acoustic epicenters determined in this manner generally locate close to mapped active faults along the Blanco Ridge, and in general differ from NEIC locations by between 4 and 71 km to the south-southwest. Using hydrophone T-wave arrivals results in a locational error (covariance matrix diagonals) of between 0.01°–0.2° in latitude and longitude, 0.1–8.0 s in origin time, at the 68% confidence interval. In Table 1, when no seismic locations are given the locations derived from the SOSUS hydrophone data were used during estimation of the CMT solution. The first two mechanisms listed in Table 1 were obtained from the NEIC Preliminary Determination of Epicenters catalog (August, 1992). The remaining mechanisms were estimated using moment-tensor inversion of the earthquakes' regional broadband waveforms (Nabelek and Xia, 1995; Braunmiller et al., 1994).

The style of faulting shown by each mechanism is consistent with the geologic structure of its location, i.e., normal faulting events occurred within the Cascadia and Gorda pull-apart basins while the strike-slip events occurred along the Blanco Ridge. Thirty-one of the Blanco Ridge strike-slip mechanisms have a component of normal motion, and indicate that the Juan de Fuca plate is the hanging wall relative to

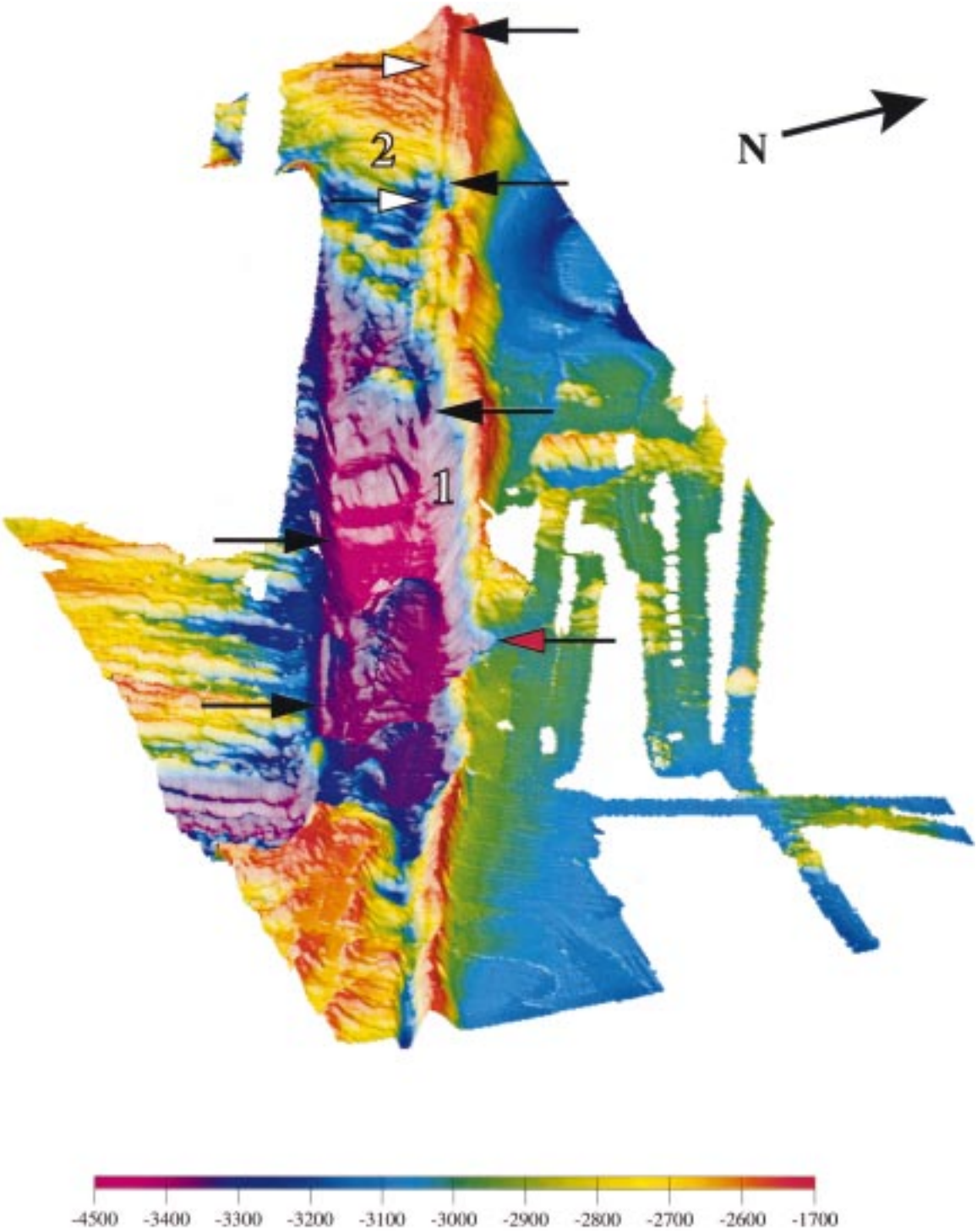

Figure 3. Three-dimensional perspective of bathymetry from the eastern half of the Blanco Ridge, Gorda Depression, and northern tip of the Gorda Ridge. Bathymetry displayed using a 200 m grid interval. Black arrows highlight probable location of active transform fault trace as it enters the northwestern section of Gorda Depression from the Blanco Ridge, and as it borders the south Gorda Depression and northern Gorda Ridge. White arrows delineate possible fault generated lineation (L2 in Figure 1) observed from bathymetry. Red arrow shows location of slump scar that cuts the Blanco Ridge. The numbers show the location of dive sites 1 and 2.

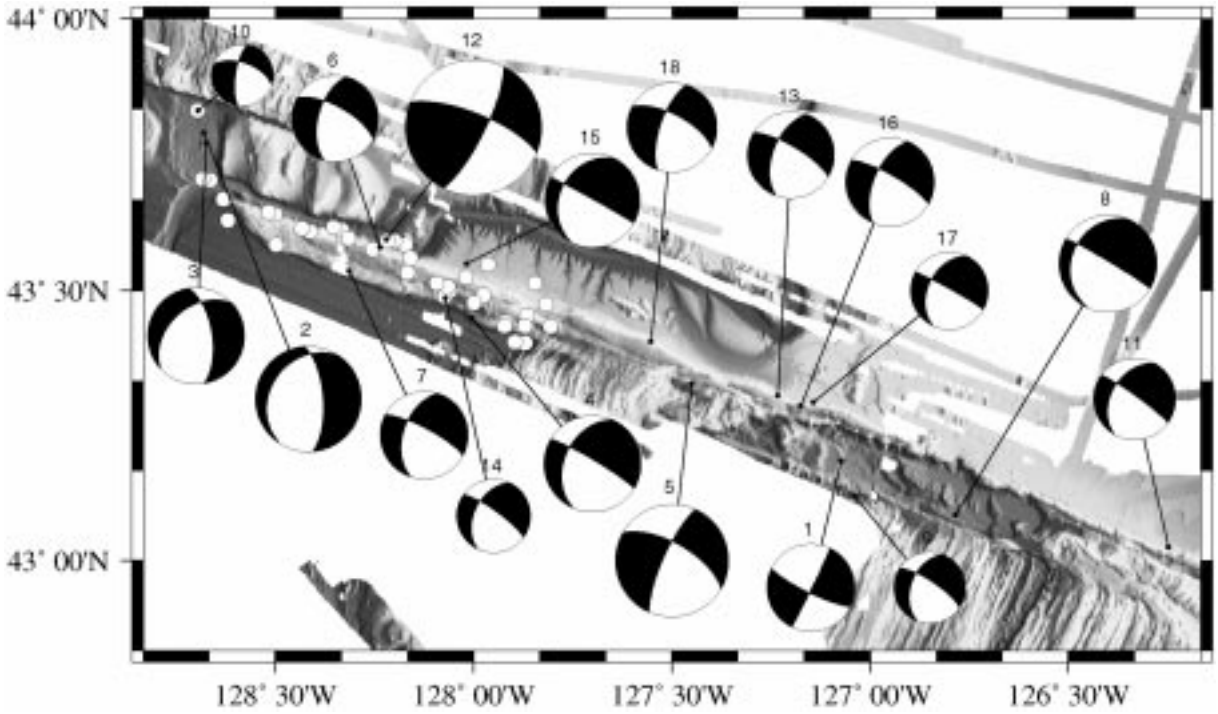

Figure 4. Recent (1992–1994) earthquakes ($4.1 \leq M \leq 6.5$), plotted on top of bathymetry of the eastern BTFZ. Earthquake focal mechanisms were estimated by the Oregon State University seismic laboratory through moment-tensor inversion of regional broadband waveform data. Earthquakes were located by the NOAA T-phase Project using acoustic earthquake data from the Navy's SOSUS hydrophone arrays. Focal mechanisms represent lower-hemisphere equal area projections, with the compressional quadrants shaded. Diameter of mechanisms is proportional to the earthquake's moment magnitude. White circles are aftershocks from the 27 October 1994 $M_w = 6.5$ (event 12) that occurred within one day of the mainshock. The earthquake locations estimated from hydrophone data generally locate close to mapped active faults along the Blanco Ridge, and differ from NEIC locations by 10 to 35 km to the south-southwest. Location and fault parameter information are listed in Tables I and II.

the Pacific plate during these events, subsiding along near-vertical fault planes. Three events (12, 22, and 35) show a component of reverse motion along the Blanco Ridge, with the Juan de Fuca plate also the hanging wall. Normal faulting events (2, 3, 9, 20, 25, 26, 36, 40, and 41) occurred along transform-oblique structures within the extensional Cascadia and Gorda Depressions, with most extensional-basin events showing a component of strike-slip motion. There are strike-slip events that border, and occur within, these extensional basins (1, 9, 8, 10, 19, 23, 27, 30, and 32), and probably are a result of strike-slip faulting entering the pull-apart basins. The strike-slip Event 11 seems to have occurred as a result of faulting along the (theoretically) inactive part of the fracture zone, and may have been caused by thermal contrasts or relative differences in intraplate stress along this section of the Juan de Fuca and Gorda plates. Overall, the mechanisms seem to indicate that the entire Blanco Ridge is undergoing predominantly strike-slip faulting with a component of normal motion, where the Juan de Fuca plate is the hanging wall and is subsiding relative to the Pacific plate. The strike-slip fault planes appear to be fairly consistent, with strikes between 290°– 310°, rakes of −116° to −178°, and most dips near vertical, but all $> 58°$.

Also shown in Figure 4 are the locations of the 27 October 1994 $M_w = 6.5$ mainshock, and 37 of its aftershocks that occurred over the following 26 hours. The NEIC (Preliminary Determination of Epicenters, October 1994) reports 2 aftershocks during this time period. Since aftershocks roughly delineate the mainshock fault-plane, it appears that about half the Blanco Ridge (∼75 km) ruptured during the 27 October 1994 mainshock. The 27 October 1994 earthquake was the largest BTFZ earthquake in four decades and had an unusually long rupture duration (Braunmiller et al., 1994), not uncommon in transform fault earthquakes (Ihlme and Jordan, 1994). The mainshock is situated in the center of the aftershock distribution, suggest-

ing the rupture may have propagated bilaterally. Also, there seems to be evidence that the earthquake ruptured a discrete fault segment since the aftershocks terminate to the west where the fault entered the Cascadia Depression, and to the east in an area of structural complexity where N–NE trending abyssal ridges intersect the transform fault at 127°40′W.

Slip vectors of the 43 CMT earthquakes along the eastern BTFZ are shown on Figure 6, summarized in Table 2, and shown on a rose diagram in Figure 7 (bottom). The slip vectors were calculated from the nodal plane information listed in Table 2 using equation (4.83) from Aki and Richards (1980) to get the x (north), y (east), and z (down) vector components. Each vector was projected onto horizontal with its azimuth representing the original plunge direction, and plotted with its length proportional to earthquake magnitude (Figure 6). The slip vectors within the extensional basins indicate a wide range of slip orientation. Some of these vectors are oblique while others parallel the trend of the transform, probably reflecting diffuse dip-slip faulting within the pull-apart basins. The slip vectors from the strike-slip earthquakes generally parallel the trend of the BR (heavy-black arrow at 111° in Figure 7). The majority of the large strike-slip vectors following eastern BTFZ transform motion oriented south (0°–9°) of the BR trend, and north of the direction of relative motion (∼N120° E) between the Juan de Fuca and Pacific plates estimated from Nuvel-1 (Demets et al., 1990). Although the slight differences in the slip vector orientations may be due to the error involved in the slip vector calculations, it is possible that slip during individual earthquakes may not necessarily be parallel to the overall transform trend or even the predicted relative plate motion. Disagreement between the direction of relative plate motion and the BR trend is to be expected since the 111° BR trend represents a mean of the trends of the individual 'lozenge-shaped' highs along the ridge. It is possible that the observed variation in slip vector orientation may actually represent slip along the variously oriented individual fault strands comprising the transform fault zone.

The maximum (P-) and minimum (T-) compression axes of the 43 earthquakes are also listed in Table 2. In general, the T-axes of earthquakes from within the Cascadia Depression are orthogonal to fault blocks within the basin, while the P-axes have variable orientations, consistent with a normal faulting regime and extension parallel to the trend of the transform. T-axes within the Gorda Depression are orthogonal to structure within the basin, and indicate NE–SW extension that is oblique to the transform trend. The Blanco Ridge P-axes have fairly consistent NW-SE trends. Figure 7 (top) shows all the P-axis trends relative to the strike of the Blanco Ridge (heavy arrow at 111°). The majority of the P-axes are horizontal and oriented between 39° and 59° to the strike of the BR. Unlike the Mendocino Transform, there should be little compression normal to the trend of the BR since (1) the oceanic lithosphere west of the Gorda Ridge moves into a space that becomes wide to the west, (2) the strike of the BTFZ is very oblique to the absolute motion of the Pacific plate, and (3) the Pacific and Juan de Fuca plates on either side of the BR are young, and relatively compliant, and therefore compression normal to the transform is reduced (Wang et al., 1997).

Single channel air-gun reflection profiles

Single channel air-gun reflection profiles were collected along the Blanco Ridge in 1969 by the Oregon State University Seismic Reflection Laboratory. The 1969 survey was the basis for a structure and tectonic study of the BTFZ (Ibach, 1981). Ibach (1981) identified a north dipping turbidite sequence (Figure 8a), along the northern base of the Blanco Ridge at longitude 127°40′ W, that had been uplifted about 300 m above the regional depth of the turbidite deposition. These turbidites are most likely spill-over deposits from the Cascadia Channel that overlie Blanco Ridge basement, and therefore suggest that the Blanco Ridge and the turbidite sequence have been uplifted. The uplifted turbidites take the form of a prominent bench on the north side of the Blanco Ridge that can be traced from 127°40′ W to 128°10′W (white arrows in Figure 2), a distance of ∼40 km along the BR with evidence of uplift. Bathymetry of the top of the turbidite bench along the northern Blanco Ridge supports the idea that there is ∼300m of uplift from east to west along the bench. Ibach (1981) interpreted the reflection profiles as indicating the presence of a south-dipping fault, with a component of reverse motion, at the base of the Blanco Ridge that was causing the uplift of the ridge and turbidites (Figure 8a). The 1969 survey also shows that along the south side of the Blanco Ridge, the Pacific plate becomes markedly deeper as it approaches the BR, with the overlying sediments showing stratigraphic thickening and structural deformation adjacent to the BR (Figure 8b). Ibach

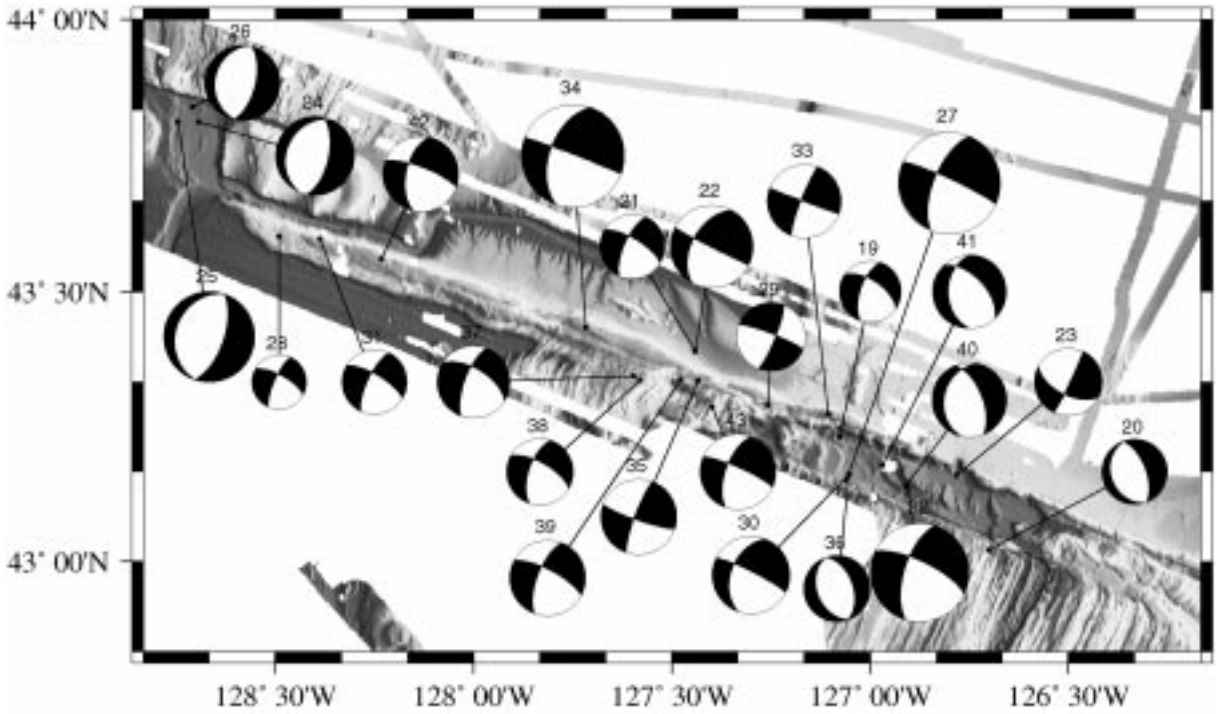

Figure 5. Recent (1995–1997) earthquakes ($3.8 \leq M \leq 5.5$), plotted on top of bathymetry of the eastern BTFZ. Mechanism and location information same as in Figure 4.

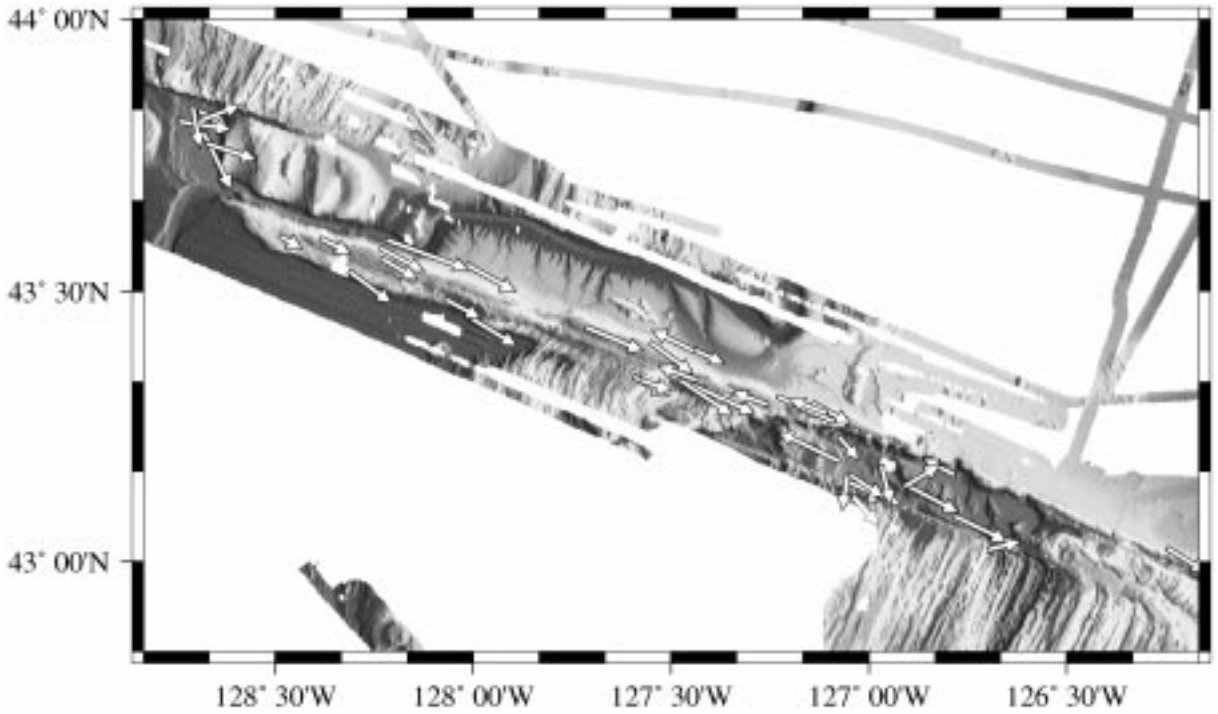

Figure 6. Orientation of earthquake slip vectors along the eastern BTFZ. Slip vectors were calculated using equation (4.83) from Aki and Richards (1980) to get the x (north), y (east), and z (down) vector components. The vector was then projected to horizontal and plotted with its length proportional to the earthquake's moment magnitude.

Table II. SOSUS location errors, first nodal planes, *P*-, *T*-axes, slip vectors

Event	No	Location error			First Nodal Plane			*P*-axis		*T*-axis		SV
	Sta	(ΔLt°)	(ΔLn°)	(ΔOT)	ϕ(°)	δ(°)	λ(°)	Az(°)	Pl(°)	Az(°)	Pl(°)	Az(°)
1	3	0.00	0.00	00.0	116	080	−178	340	009	194	080	295.8
2	4	0.01	0.02	01.4	214	028	−055	238	064	099	021	154.4
3	4	0.05	0.06	05.0	351	063	−124	213	058	104	012	128.7
4	4	0.02	0.01	01.8	301	084	−131	175	037	062	027	115.1
5	4	0.07	0.07	06.3	300	065	−166	160	027	254	009	114.6
6	4	0.09	0.18	08.1	299	068	−146	160	039	065	006	118.2
7	4	0.02	0.04	01.5	298	078	−140	166	036	062	018	126.9
8	3	0.00	0.00	00.0	301	087	−116	186	043	053	036	115.7
9	3	0.00	0.00	00.0	304	076	−135	172	041	066	018	138.0
10	3	0.00	0.00	00.0	290	058	−159	146	036	242	009	115.8
11	4	0.07	0.06	04.5	306	084	−132	180	036	069	027	121.6
12	4	0.08	0.14	08.8	292	073	166	159	002	252	022	109.9
13	4	0.03	0.02	03.0	301	075	−145	166	035	067	012	112.3
14	4	0.04	0.04	02.7	306	079	−136	176	038	069	021	118.7
15	4	0.06	0.08	05.4	299	089	−121	182	038	056	037	118.9
16	4	0.001	0.001	00.01	300	078	−150	165	030	069	011	113.8
17	4	0.001	0.001	00.01	299	087	−134	173	033	063	028	118.9
18	6	0.02	0.04	03.4	298	067	−157	158	032	249	001	126.4
19	6	0.04	0.05	06.3	304	061	−150	160	041	252	002	160.0
20	4	0.03	0.03	05.7	339	062	−091	247	073	070	017	075.4
21	4	0.01	0.02	01.8	301	071	−159	163	028	073	000	114.9
22	3	0.00	0.00	00.0	117	088	141	169	024	065	028	296.5
23	3	0.00	0.00	00.0	117	058	−176	336	024	075	019	297.6
24	3	0.00	0.00	00.0	012	062	−096	269	072	106	017	068.3
25	4	0.003	0.004	00.2	019	064	−090	289	071	110	019	098.6
26	4	0.03	0.02	01.4	014	062	−088	289	073	103	017	170.4
27	4	0.01	0.01	00.5	295	084	−155	161	022	066	013	113.2
28	4	0.07	0.05	03.2	299	070	−165	160	024	252	004	118.8
29	3	0.00	0.00	00.0	291	083	−010	155	012	246	002	199.8
30	4	0.04	0.03	02.2	297	083	−136	168	035	061	023	123.1
31	4	0.04	0.03	01.8	301	072	−162	341	074	105	009	210.6
32	4	0.04	0.02	01.9	296	072	−153	159	031	066	005	117.8
33	4	0.02	0.01	01.1	111	089	173	156	004	066	006	290.9
34	6	0.02	0.02	00.9	291	088	−143	162	026	059	023	112.5
35	6	0.01	0.01	00.6	109	082	171	155	001	064	012	290.2
36	6	0.02	0.02	00.9	341	050	−089	263	085	069	005	188.6
37	6	0.01	0.01	00.6	302	061	−157	158	036	252	006	197.7
38	6	0.02	0.02	00.7	300	068	−151	160	035	068	003	108.7
39	6	0.05	0.05	02.4	298	073	−157	161	028	069	004	124.2
40	5	0.01	0.03	00.9	338	062	−108	212	068	082	015	059.1
41	6	0.02	0.02	00.9	316	057	−118	174	065	066	008	166.1
42	6	0.02	0.02	00.2	291	076	−147	156	034	058	011	120.0
43	6	0.06	0.07	03.5	294	081	−153	160	026	064	012	109.4

(1981) interpreted this section as a south dipping fault, with evidence of ~300 m of uplift of the Blanco Ridge relative to the abyssal plain sediments, as indicated by an uplifted sediment wedge overlying the BR south base. Figure 8b also shows the interpretation of a south dipping fault along the north BR base. The original 1969 profiles have been reviewed further (V. Kulm, pers comm., 1997). In contrast to the findings of Ibach (1981), the 1969 reflection profiles show no evidence of a south dipping fault beneath the turbidite sequence along the northern BR. As indicated by the interpretation in Figures 8a and 8b, however, the profiles seem to indicate that the BR basement does dip to the north on the north side of the ridge, dips to the south on the south side of the ridge, and that there is a south dipping fault at the toe of the uplifted sediment wedge along the southern BR. Furthermore, the north dipping basement on the north side of the BR is overlain nonconformably by the turbidite sequence, with either a vertical or (possibly north dipping) dip-slip fault apparent at the toe of the turbidite bench. The L1 and L2 lineations (L1 and L2 in Figure 1; white arrows in Figures 2 and 3) at the north and south base of the BR may be the surface expressions of the faulting at the toe of the turbidite sequence.

Submersible and ATV observations

During late August and early September of 1994, a cruise sponsored by the National Undersea Research Program aboard the R/V *Laney Chouest* resulted in three deployments of the U.S. Navy's Advanced Tethered Vehicle (ATV), and one deployment of the U.S. Navy's DSV *Turtle* at sites along the Blanco Ridge (Figures 2 and 3). The dives on the Blanco Ridge resulted in approximately 67 hours of video, 1000 still photographs, 57 rock samples, and 10 sediment cores. In general, the Blanco Ridge is a strongly tectonized feature exposing a mixture of rock types with both crustal and subcrustal affinities (Koski et al., 1994). The upper slopes are partly mantled by sedimentary breccia and loose rock debris; the lower slope on the north side is draped with sediment, while the southern lower slope is sediment free. There was abundant evidence of mass wasting and slumping observed on the north facing slopes suggesting that active faulting is concentrated on the north flank of the ridge. Although no active venting was observed along the Blanco Ridge, hydrothermally altered and veined basalt samples were obtained from the ridge flank adjacent to the Gorda Depression. Rock samples obtained from shoaler parts of the ridge to the west of the Gorda Depression include gabbro and basalt with greenschist facies mineral assemblages (Koski et al., 1994). A detailed description of the ATV/submersible surveys and collected samples is presented in the following sections.

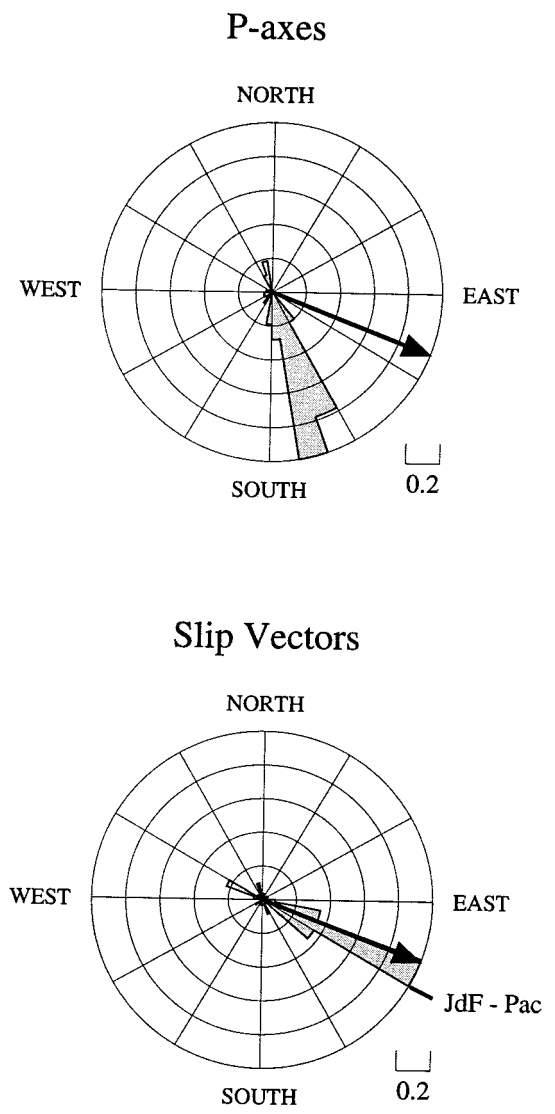

Figure 7. Rose diagrams showing orientation of earthquake P-axes (top) and slip vectors (bottom). Heavy black arrows on each diagram represents the BTFZ trend (~111°). In general, *P*-axes are oriented between 39° to 59° to the strike of the transform. The majority of large horizontal slip vectors following eastern BTFZ transform motion are oriented between the trend of the Blanco Ridge and the Juan de Fuca-Pacific plate relative motion vector (~N120°E).

To obtain the ATV/submersible's approximate location, three methods were concurrently used:

(1) ATV/submersible depth in comparison to bathymetry, (2) ATV/submersible locations relative to GPS ship locations using slant range, and (3) ATV/submersible heading and sonar which gave information on direction to, and steepness of, nearby terrain. Thus vehicle locations on the seafloor are probably good to about 200 m.

Blanco Ridge geology – Site 1

Figure 9 shows the tracklines, bathymetry, and geologic interpretation of the first ATV dive (Dives 1A and 1B) of the 1994 cruise done along the northwestern wall of the Gorda Depression and base of the Blanco Ridge. Table 3 lists the sample locations and petrology of the samples taken along the track. Prior to the field work performed on the *Laney Chouest*, the only samples to have been recovered from the Blanco Ridge were a suite of gabbros, diabases, basalts (greenstones), and greenstone breccias dredged in 1985 from this portion of the ridge adjacent to the Gorda Depression (Hart et al., 1990). All samples found during the 1985 survey had been hydrothermally altered under greenschist conditions, with multistage fragmentation, brecciation, and vein-filling mineral precipitation ($>$ 500 °C sulfides, 350°–500 °C carbonates and zeolites, $<$ 200 °C quartz-chert) accompanying hydrothermal activity.

The base of the ridge within the Gorda Depression itself is heavily sedimented, but changes to a talus slope of basalt and diabase breccias after ∼600 m climb up from the basin (Dive 1A; Figure 9 and Table 3). Approximately 300 m (2640 m depth) above the talus slope was a steep (∼60°) scarp face of highly jointed and fractured diabase with a very-light sediment cover. The diabase appeared to have originated from fracture-bounded dikes within the scarp. Basalt was present in places, but when sampled, appeared to be talus blocks rather than from the outcrop itself. The steep, massive, and highly fractured appearance of the scarp face suggests it is an expression of the active, transtensional strike-slip fault boundary of the Gorda Depression. The scarp continued for ∼500 m (2155 m depth), changing abruptly to a shallow, southwest dipping sediment-covered slope that continued to the top of the ridge. No outcrops were apparent in the sediment, but an angular basalt cobble was sampled near ridge's summit (2147 m depth).

A short ATV survey (Dive 1B; Table 3) was then conducted 2 km to the east. As before, a steep highly-fractured scarp face composed of diabase was encountered. Veins of white material were observed (and sampled) within the brecciated diabase. Petrographic analysis showed two generations of veining; the first veins are narrow and composed of fibrous amphibole. The second are larger, more extensive, and lower temperature carbonate veins.

Site 2

Figure 10 shows the trackline, bathymetry, and geologic interpretation of ATV dives at the second site along the south-central portion of the Blanco Ridge. The sample locations, depths, and petrology are summarized in Table 4. The dive was broken into two portions. Dive 2A covered the north-northeast trending abyssal hills south of the active transform fault trace, and Dive 2B targeted the Blanco Ridge. The Blanco Ridge portion of the dive was selected at this particular location because of a possible small ($<$ 1 km) step in the fault trace apparent from the bathymetry (Figure 10).

Dive 2A began at 2546 m depth within a heavily sedimented basin. The ATV maintained a heading (∼315°) perpendicular to the trend of the ridge-forming abyssal hills. The northeast-trending abyssal hills form a series of *én echelon* ridges that bend to the east as they approach the transform fault (Figure 1). Folding of the ridges is probably a result of drag due to resistance of motion along the strike-slip fault. The dive crossed three ridges. At the base of each were basalt talus fields that changed to massive basalt scarps (sloping southeast ∼45°) farther upslope. The tops of each ridge, like the basins between them, were heavily sedimented with no outcrops observable. The ridges rise to about 100–150 m above the basins. The basalts sampled at each basal scarp were highly fractured pillows composed of slightly altered porphyritic basalts. These basalts have phenocrysts of plagioclase and olivine, and some carbonate veining. The scarps are interpreted here as recently active faults since they have little sediment cover and cut the youngest seafloor sediment. These faults are probably reactivated normal faults, which are present in the ∼2.3 Ma Pacific plate crust (∼30 km off-axis) from relict Gorda Ridge spreading fabric. Abyssal hill bounding normal faults have been shown to be active up to 35 km (∼1 Ma) off-axis of the East Pacific Rise (Macdonald et al., 1996). Since the abyssal ridges take an eastern bend near the transform fault, it could be that drag faulting and uplift of the abyssal ridges occurs due to strike-slip motion of the transform fault and the ap-

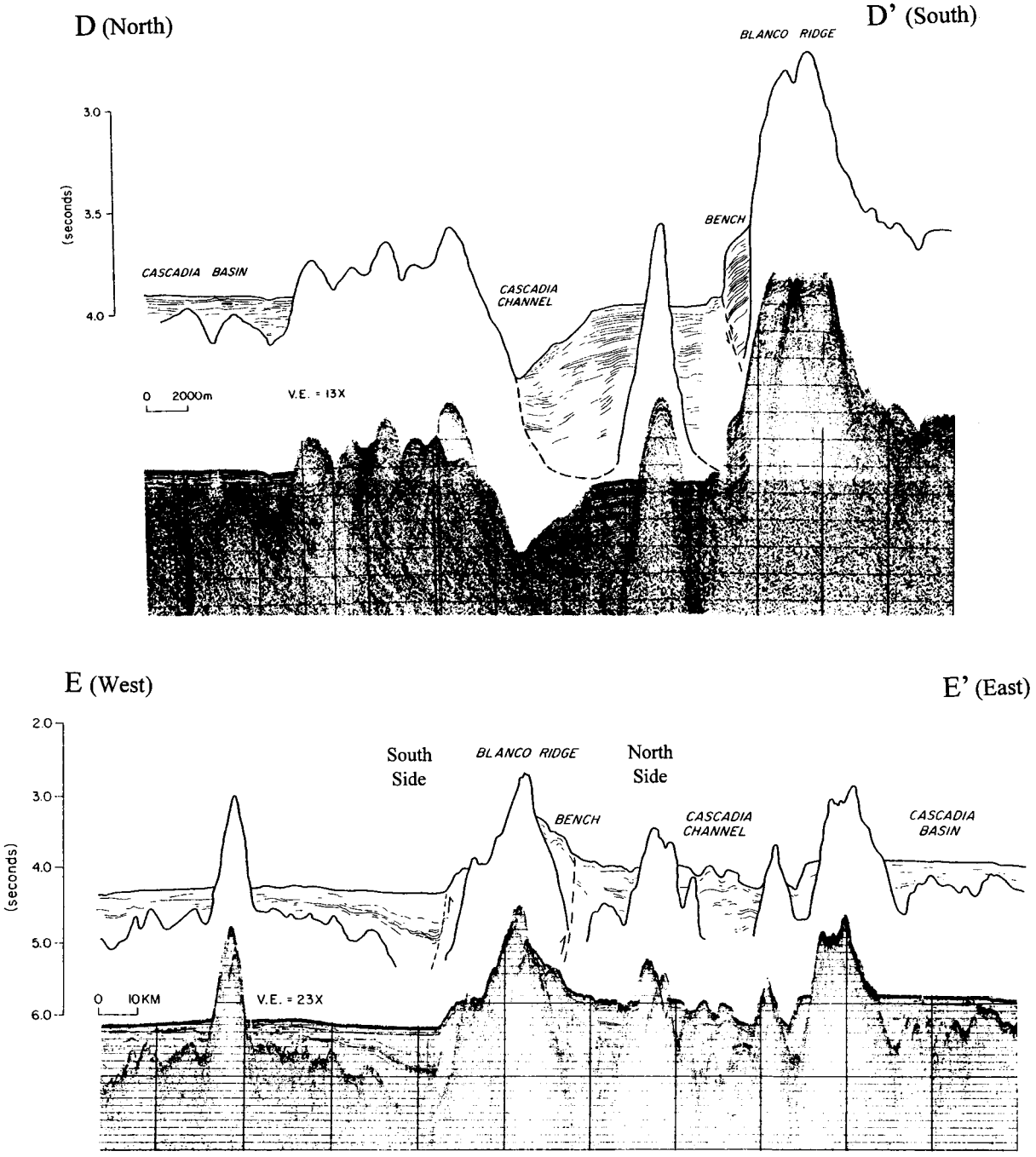

Figure 8. Diagrams showing single-channel airgun reflection profiles and interpretations from Ibach (1981). (a) shows north-south profile across the Blanco Ridge (at 127°40′ W), and interpretation (profile D-D′ in Figure 1). The profile illustrates the uplifted and faulted nature of the Blanco Ridge as shown by the uplifted turbidite bench. Ibach (1981) interpreted the profile to show a south-dipping fault along the northern Blanco Ridge, which is not necessarily supported by the data. (b) shows northeast-southwest profile paralleling the Blanco Ridge and interpretation (profile E-E′ in Figure 1). Profile again illustrates the faulted and uplifted nature of the Blanco Ridge, and shows uplifted sediment wedges on both the north and south sides. On the south side of the Blanco Ridge there is evidence for subsidence of the Pacific plate and overlying sediments.

Table III. Dives 1A and 1B: Site 1 borda depression: sample locations, depths, and petrologic description – 27 August 1994

Sample	Time	Location		Depth	Descrip.	Geologic setting
	UTM	Lat(°,′)	Lon(°,′)	(m)		
	Dive 1A: Gorda Depression					
1	23:20	43 15.04	−127 05.02	3125	Diabase	Talus block from Gorda Dp, BR base
2	00:43	43 15.55	−127 05.90	2954	Diabase	Talus block moderate south slope BR
3	01:07	43 15.71	−127 05.95	2884	Basalt	Block from talus pile, light sediment
4	01:22	43 15.75	−127 05.96	2841	Diabase	Talus block, moderate slope
5	01:55	43 15.76	−127 05.96	2769	Dia. Brec.	Talus block on steep slope
6	02:17	43 15.77	−127 05.96	2640	Diabase	Talus block at base of steep scarp
7	02:31	43 15.77	−127 05.96	2613	Diabase	Talus block up steep scarp
8	02:48	43 15.82	−127 05.97	2540	Basalt	Debris from base of steep outcrop
9	03:01	43 15.89	−127 05.98	2485	Diabase	In situ block from steep scarp
10	03:13	43 15.91	−127 05.98	2470	Diabase	In situ block from steep scarp
11	03:51	43 15.93	−127 05.98	2265	Diabase	Talus block along steep scarp
12	04:00	43 15.95	−127 05.98	2241	Diabase	In situ block from steep scarp
13	04:12	43 15.96	−127 05.98	2213	Diabase	In situ block from sheared scarp face
14	04:22	43 15.97	−127 05.98	2183	Diabase	In situ block from sheared scarp face
15	04:36	43 16.08	−127 05.96	2155	Basalt	Talus from debris flow on scarp
16	05:03	43 16.22	−127 05.85	2147	Lost	Pillow shape sample, ridge summit
	Transit to new survey site downslope Blance Ridge					
	Dive 1B: Gorda Depression					
17	14:38	43 15.13	−127 04.32	3168	Diabase	Talus block from flow on steep slope
18	15:15	43 15.21	−127 04.25	2997	Diabase	In situ block, fractured scarp face
19	15:38	43 15.31	−127 04.22	2894	Diabase	In situ block, fractured scarp face
20	16:05	43 15.40	−127 04.12	2817	Diabase	In situ block, fractured scarp face

Table IV. Dives 2A and 2B: Site 2 Abyssal Hills and East Blanco Ridge sample locations, depths, and petrologic description–30 August 1994

Sample	Time	Location		Depth	Description	Geologic setting
	UTM	Lat(°,′)	Lon (°,′)	(m)		
	Dive 2A: Abyssal Hills South of Blanco Ridge					
1	22:03	43 20.85	−127 36.01	2546	Porphy. Basalt	Talus block from slope base
2	22:17	43 20.95	−127 36.05	2470	Porphy. Basalt	In situ block, fractured scarp face
3	01:20	43 21.13	−127 36.24	2543	Porphy. Basalt	Pillow basalt, fractured scarp face
4	02:45	43 21.22	−127 36.30	2482	Porphy. Basalt	In situ block, fractured scarp face
5	02:49	43 21.48	−127 36.45	2482	Porphy. Basalt	In situ block, fault scarp face
6	03:15	43 21.50	−127 36.49	2445	Porphy. Basalt	In situ block, top of fault scarp
7	04:38	43 21.55	−127 36.52	2423	Porphy. Basalt	Pillow basalt, top of fault scarp
	Transit north to new survey site, base of Blanco Ridge					
	Dive 2B: East Blanco Ridge					
8	18:54	43 22.94	−127 36.82	2377	Porphy. Basalt	Talus block, Blanco Ridge base
9	22:33	43 23.30	−127 37.50	2375	Porphy. Basalt	Talus block, Blanco Ridge base
10	22:45	43 23.29	−127 37.56	2375	Porphy. Basalt	Talus block, Blanco Ridge base
11	23:33	43 23.20	−127 37.66	2363	Basalt Breccia	Rock fragment near BR summit
12	01:23	43 22.94	−127 38.22	2302	Gabbro Mylo.	Rock fragment near BR summit

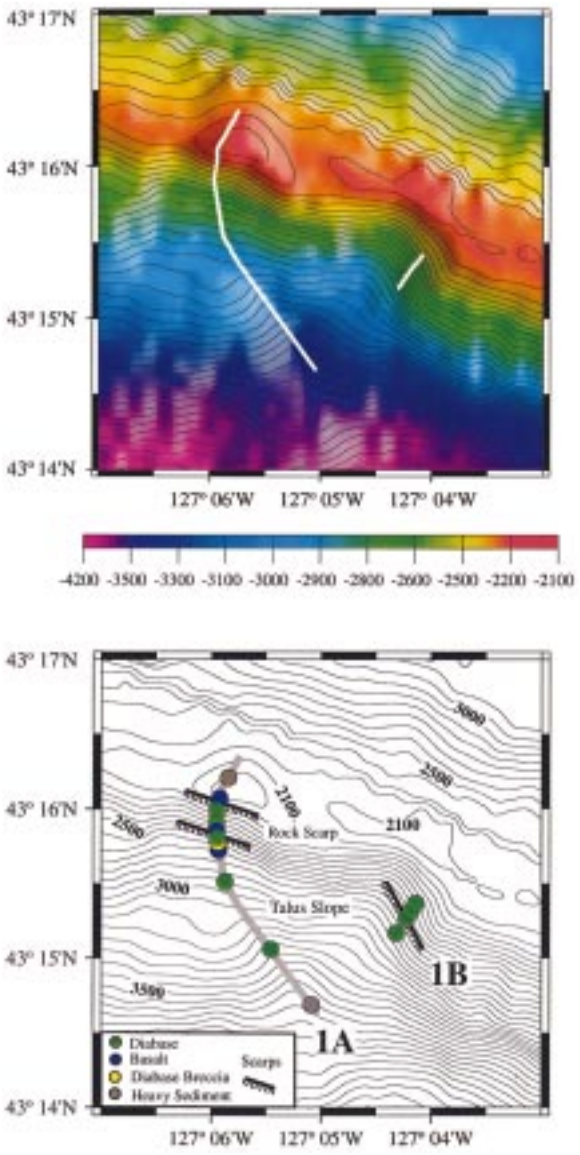

Figure 9. Seafloor survey site 1 bathymetry (top), submersible tracklines (white and grey lines), sample locations and their petrology, and observed geologic structure. Location of survey site shown on Figure 3. Bathymetry displayed (and in Figures 10–12) using a 100 m grid interval.

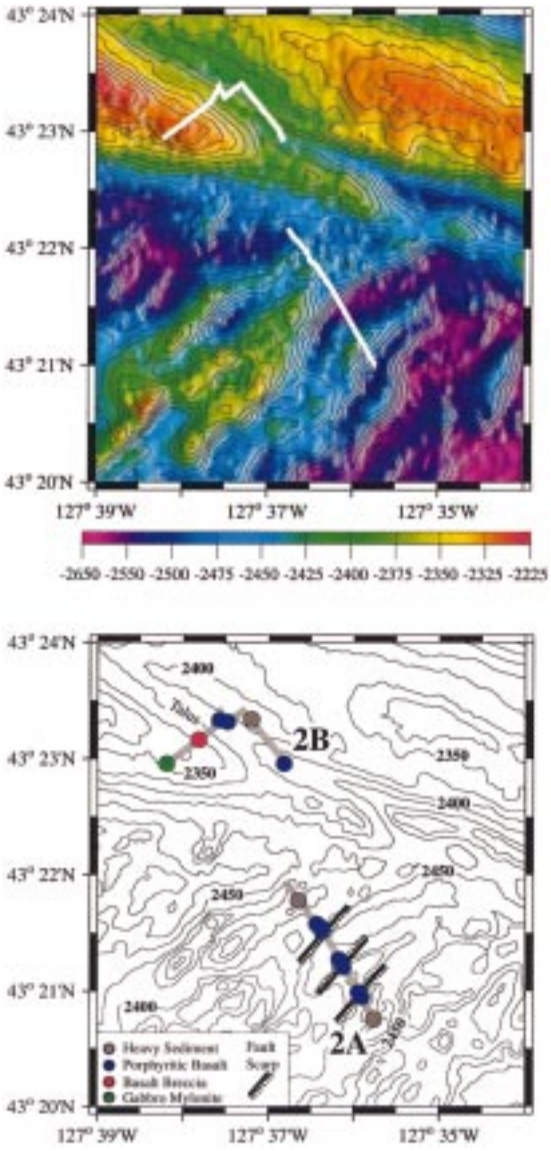

Figure 10. Seafloor survey site 2 bathymetry (top), submersible tracklines (white and grey lines), sample locations and their petrology, and observed geologic structure. Location of survey site shown on Figure 3.

parent uplift of the Blanco Ridge, respectively. These ideas remain speculative, however, because it is not possible to directly estimate the sense of motion on these faults since the dive data are not conclusive, and there is no seismic-reflection data available from this location.

Dive 2B began in a saddle (depth ~2400 m) between two small Blanco Ridge segments (Figure 10). The dive tracked oblique to the saddle (~315°) before changing course up the north face and to the summit of the southwestern ridge segment. The saddle was heavily sedimented and a basement outcrop was not found. The base of the southwest ridge segment (depth ~2377) had an extensive apron of porphyritic-basalt talus blocks ranging in size from ~10 to 20 cm. The basalts had large phenocrysts of plagioclase and olivine (with carbonate veining) similar to the abyssal hills to the south. The talus slope continued to a depth of 2315 m (~62 m), where the ridge became cov-

ered with a basalt gravel pavement with little sediment cover. Locally, outcrops of porphyritic basalt were observed protruding through the pavement. Along the northern ridge face, fragments of a basalt breccia (2360 m) and a recrystallized mylonite block (2300) were found. The mylonite is a fine-grained, foliated, and recrystallized gabbro with late-stage chlorite veins that cut across the foliation. This was the only mylonite to be found among the petrologic samples collected during the 1994 dive series. The north face of this ridge segment remained covered with gravel-sized pavement until the ridge crest (depth = 2290 m), where the sediment cover again became thick.

Site 3

Figure 11 shows the trackline, bathymetry, and geologic interpretation of ATV dives 3A and 3B at site 3 along a north central portion of the Blanco Ridge. The sample locations, depths, and petrology are summarized in Table 5. The dive track was chosen here because it traverses the north side of the ridge along an apparent slump scar that cuts the ridge. This track resulted in a good compositional view of the Blanco Ridge from base to summit. The slump block appears to be the NW-SE trending linear ridge northeast of the slump scar (marked with an 'S' in Figure 1). The distance between the scar and debris suggests that the slump scar is on the Pacific plate, the block is on the Juan de Fuca plate, and the two have been moved apart by motion along the transform. The horizontal distance between the western edge of the slump scar and block is ~25 km, and with a long-term plate motion rate of ~5.5 cm/yr across the BTFZ, suggests that the slump occurred ~454 ka. This age would explain the large amount of sediment covering the slump scar basin. Also, this suggests the ATV track up the steep scarp face traversed Pacific plate crust.

Dive 3A began within thick sediment cover at the base of the Blanco Ridge (depth of 2961 m). The ATV heading of 180°–190° took the vehicle over a low ridge that has formed at the edge of the slump scar, then into a basin scoured at base of the scar. This low ridge is the surface expression of the BR parallel lineation identified from bathymetry in Figure 1. We speculate that the lineation may be a dip-slip fault that has exhibited displacement since the time of the slump, and thus has formed a ridge at the base of the slump scar. Unfortunately, sediment cover was thick throughout this section of the dive, and no outcrops or rock fragments were observed. At the base of the headwall of the scar (2939 m), porphyritic basalt, diabase, and gabbro (heterolithic) breccia were sampled from a steep, heavily sedimented scarp face that continued 2436 m (~500 m), where the ridge became a near-vertical rock scarp. The scarp face is a massive wall of highly fractured gabbro ~80 m high. Although diabase and basalt talus blocks were sampled along the scarp, the two clear outcrop samples taken from the scarp face were a gabbro and a gabbro breccia. The gabbro shows quartz and carbonate veining that took place prior to brecciation. No slickensides or other micro-structural features were observed, therefore it is not clear whether the scarp is a slump surface or the active transform trace. At the crest of the scarp, the

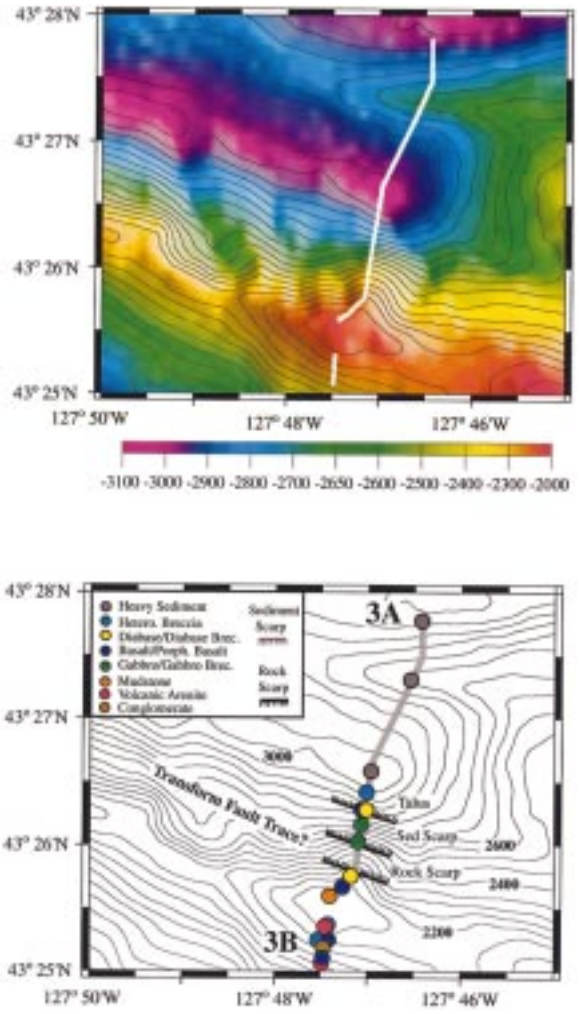

Figure 11. Seafloor survey site 3 bathymetry (top), submersible tracklines (white and grey lines), sample locations and their petrology, and observed geologic structure. Location of survey site shown on Figure 2.

Table V. Dives 3A and 3B: Site central Blanco Ridge sample locations, depths, and petrologic description–1 September 1994

Sample	Time	Location		Depth	Description	Geologic setting
	UTM	Lat(°,′)	Lon (°,′)	(m)		
	Dive 3A Slump Scar - north flank Blanco Ridge					
1	22:04	43 26.55	−127 47.01	2939	Hetero. Breccia	Talus debris base of BR
2	01:00	43 26.39	−127 47.01	2927	Diabase Breccia	Rock fragment off sed. scarp
3	01:04	43 26.38	−127 47.01	2927	Basalt	Rock fragment off sed. scarp
4	01:25	43 26.34	−127 47.02	2866	Hetero. Breccia	Talus block, steep sed. scarp
5	02:43	43 26.21	−127 47.10	2686	Gabbro Breccia	Talus block, steep sed. scarp
6	03:16	43 26.02	−127 47.11	2436	Gabbro	In situ block, vertical scarp face
7	03:42	43 25.84	−127 47.12	2334	Diabase	Talus block from debris flow
8	03:56	43 25.75	−127 47.26	2299	Basalt	Rock fragment, flank of BR
9	03:46	43 25.62	−127 47.41	2110	Mudstone	In situ block from BR summit
	Transit south to new servey site, south flank of Blanco Ridge					
	Dive 3B south flank Blanco Ridge					
9	07:43	43 25.08	−127 47.47	2302	Volcanic Arenite	Rock fragment, south BR slope
10	07:56	43 25.10	−127 47.48	2290	Porphy. Basalt	Talus block, south slope BR
11	08:07	43 25.21	−127 47.47	2375	Conglomerate	Talus block, south slope BR
12	08:42	43 25.26	−127 47.47	2220	Basalt Breccia	Talus block, south slope BR
13	09:11	43 25.26	−127 47.46	2159	Porphy. Basalt	Rock fragment near BR summit
14	09:30	43 25.39	−127 47.46	2128	Volcanic Arenite	Rock fragment near BR summit
15	09:41	43 25.45	−127 47.45	2128	Basalt Breccia	Large block at BR summit

ridge slope shallowed considerably (still dipping N–NE) and became mantled by a gravel pavement (light sediment cover) up to the Blanco Ridge summit. Fragmented blocks of basalt and diabase were sampled in this region, likely reflecting basement composition beneath the sediment. The Blanco Ridge summit was reached at a depth of 2110 m, where a mudstone was sampled.

Dive 3B was a brief traverse up the south side of the Blanco Ridge (Figure 11). The first sample (at 2302 m) was a volcanic arenite cobble collected from a light sediment/gravel pavement seafloor dipping steeply to the south. Further upslope, porphyritic basalt and basalt breccia blocks were sampled as random fragments within the gravel pavement, again likely reflecting basement composition along this section of the ridge. Samples of conglomerate (depth of 2277 m) and volcanic arenite (depth of 2128 m) were also collected upslope along the south face. The conglomerate is composed of rounded calcarious-mudstone clasts within a matrix containing planktonic foraminifera, while the arenite is composed of basalt fragments and palagonite clasts. The presence of the mudstone, conglomerate, and arenite at the top of the ridge is intriguing, although these sedimentary rocks probably formed locally. The conglomerate and arenite samples were taken from what appeared to be a debris flow originating at the ridge summit. The gravel pavement and light sediment cover continued along the south face of the ridge until the dive was terminated near the summit (depth of 2128 m).

Site 4

The bathymetry, trackline, and geologic interpretation of the submersible Dive 4 at site 4 using the U.S. Navy DSRV *Turtle* is shown in Figure 12. The approximate sample location, depths, and petrology are summarized in Table 6. This location was selected to provide not only a view of the shoalest portion of the Blanco Ridge but also the geologic section of the south-facing ridge scarp. Because the submersible could not be tracked precisely, a constant effort was maintained throughout the dive to traverse the steepest slope to ensure the Blanco Ridge summit was reached. The dive began along the Blanco Ridge south face (2349 m depth), which had a surface of gravel pavement with little or no sediment cover. The first sample col-

lected was a brecciated gabbro block (∼10 cm) from a pile of talus along the ridge slope. The ridge surface remained a gravel pavement with ubiquitous talus blocks to a depth of 2281 m where another gabbro talus block was sampled. This gabbro had oriented, plagioclase-rich zones suggestive of a cumulate origin. At the break of slope at the ridge summit (depth of 2138 m) another gabbro talus block was sampled. The gabbro was undeformed, showing no signs of brecciation. The submersible then remained along the ridge crest crossing a set of large fractures oriented approximately parallel to the strike of the transform (depth of 2141 m). Within these fractures a sample of brecciated cumulate gabbro was obtained. This deformed gabbro was characterized by variably rounded clasts within a granulated matrix. Continuing east-southeast along the ridge peak, the ridge surface remained a gravel pavement with little or no sediment and widely distributed talus blocks (∼10–100 cm in size). Along this portion of the ridge summit, there were many crabs, starfish, clams, and rays. Another undeformed gabbro was sampled (depth = 2050 m) further along this track from a ridge summit outcrop. The dive ended along the top of the Blanco Ridge at a depth 1972 m (Figure 12), a few hundred meters southwest of the ridge's shoalest point (depth 1870 m). A porphyritic basalt block was taken here from a small talus pile that was on top of the gravel pavement. The basalt talus block was likely derived from an outcrop near the ridge summit, perhaps emplaced through fracturing and seismic shaking.

Sea-surface gravity and magnetics

A sea-surface magnetic and gravity profile collected in 1988 across the Blanco Ridge was obtained from the National Geophysical Data Center (Figure 13). The profile crosses the ridge at 128°10′ W, and is roughly orthogonal to the strike of the transform. The profile also happens to cross the Blanco Ridge where the beginning of magnetic isochron 3 is juxtaposed in both the Juan de Fuca and Pacific plates (Wilson, 1993). Thus the plate ages (∼4.2 Ma) and magnetic polarity should roughly be equal at this longitude on either side of the transform. Furthermore, seismic refraction studies along the southern Juan de Fuca (McDonald et al., 1994) and northern Gorda Ridges (Bibee, 1986) indicate that relative thicknesses of the upper oceanic-crust sections are roughly the same, therefore adjacent portions of the Juan de Fuca and Pacific plates along the Blanco Ridge should also have similar crustal layer thicknesses. The vertical dashed lines on the profiles in Figure 13 represent the location of the transform fault trace estimated from bathymetry and seafloor mapping efforts. The magnetic profile (representing total field minus reference) over the Blanco Ridge shows a distinct region over the fault zone, with a magnetic anomaly high. This signal might be generated by a greater relative basement uplift of the Blanco Ridge on the Pacific plate side, with the magnetic lows over the BR north and south flanks caused by thick (∼2 km; Embley, 1985) turbidite sequences. A map view of northeast Pacific ocean magnetic anomalies (total field minus reference) compiled by Riddihough (1984) shows a 200 nT anomaly at the BR as well, and also indicates that the anomaly parallels the strike of the BR south flank.

Cross sections of the free-air and Bouguer anomalies are also shown in Figure 13. The sea-surface free-air gravity data along this profile was directly available from NGDC. The free-air anomaly indicates a high over the ridge and a pronounced low along the BR south flank. A map view of free-air anomaly was also compiled by Riddihough et al. (1982) for the entire region. The map view shows the same anomaly shape as the profile, and indicates that the high and low anomalies parallel the strike of the ridge crest and ridge south flank, respectively. The Bouguer anomaly profile was estimated for this study from the free-air gravity by removing the effects of bathymetry and the water column along the profile. Densities of 2.7 g cm^{-3} (basalt) and 1.03 g cm^{-3} (water) were used. Since the plate ages on either side of the transform at this longitude are roughly equal, gravity calculations were not corrected for lithospheric density contrasts across the fault. The estimated Bouguer anomaly profile indicates a greater negative anomaly (mass deficit) under the south side of the BR, and smaller negative anomalies along the north and south BR flanks. Negative Bouguer anomalies indicate the BR may be compensated in an Airy fashion by some low density body. A strong positive Bouguer anomaly would have suggested a regional compensation mechanism for the Blanco Ridge and would likely require a flexural model of formation (e.g., Kane F.Z. from Abrams et al., 1988; Clipperton and Siqueiros F.Z. from Pockalny et al., 1997). The negative anomalies on the flanks are probably due to the thick turbidite sequences of density ∼2.45 g cm^3 (Embley, 1985). The larger negative anomaly under the ridge is possibly due to a narrow (∼5 km) low-density zone beneath the BR, which seems to be centered along the Pacific

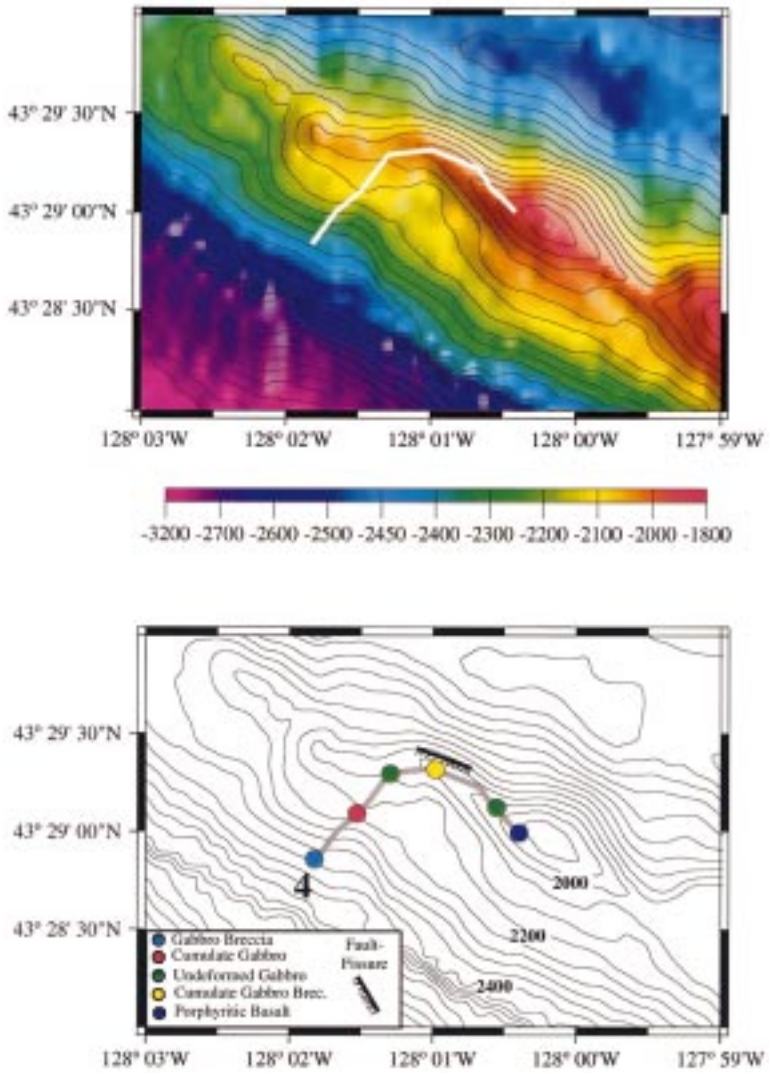

Figure 12. Seafloor survey site 4 bathymetry (top), submersible tracklines (white and grey lines), sample locations and their petrology, and observed geologic structure. Location of survey site shown on Figure 2.

Table VI. Dive 4: Site 4 Blanco Ridge South Flank and summit sample locations, depths, and petrologic description–31 August 1994

Sample	Time	Location		Depth	Description	Geologic setting
	UTM	Lat(°,′)	Lon (°,′)	(m)		
	Dive 4: Blanco Ridge South Flank					
1	11:55	43 28.9	−128 01.9	2349	Becciated Gabbro	South base of BR talus
2	12:52	43 29.1	−128 01.5	2281	Cumulate Gabbro	Talus along BR south face
3	13:44	43 29.3	−128 01.4	2138	Undeformed Gabbro	Talus from ridge top
4	14:05	43 29.4	−128 01.0	2141	Cumulate Gab. Brec	In situ block within parallel fractures along ridge peak
5	15:25	43 29.1	−128 00.7	2050	Undeformed Gabbro	Talus at ridge summit
6	16:02	43 28.9	−128 00.5	1972	Pophyritic Basalt	Talus block from BR summit

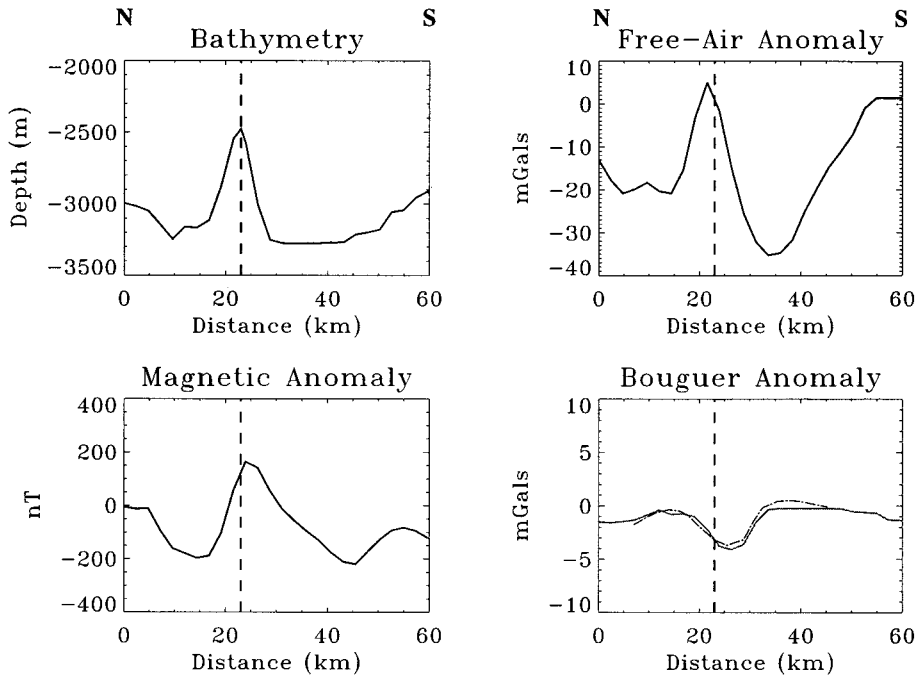

Figure 13. North-south profile of bathymetry (top left), free-air sea-surface gravity (top right), magnetic profile (bottom left), and Bouguer anomaly (bottom right) across the Blanco Ridge. Location of profiles shown as line G-G′ in Figure 1. Data from profile collected by NOAA in 1988. Dashed line in each profile represents the location of the active transform fault estimated from bathymetry and seafloor mapping efforts. Magnetic profile represents observed total field minus 1985 International Geomagnetic Reference Field. Bouguer anomaly (grey line) estimated from free-air by removing bathymetric and water column effects. Dashed line shows model of Bouguer anomaly produced from parameters listed in text.

plate (south) side of the transform. In order to test this hypothesis, a forward model of the free-air anomaly was estimated using a simple two-dimensional crustal model. The negative Bouguer anomaly was modeled (Figure 13, bottom right) assuming a 10 km rigid plate thickness (constrained by earthquake focal depths), 1.5 km thick ($\rho = 2.45$ g cm^{-3} for the entire section) sediment wedges along the BR flanks, and a 5 km wide, 3 km thick, and 1 km deep low-density ($\rho = 2.5$ g cm^3) body beneath the BR itself.

The gravity model proposed is non-unique, but a low-density body at depth along the transform fault would account for the negative Bouguer anomaly. Furthermore, a low-density body is consistent with serpentinite intrusion along the fault. Negative Bouguer anomalies have previously been observed along the Tamayo Transform ridge (Kastens et al., 1979) and were modeled assuming a low-density serpentine body at depth beneath the transform using density values of 2.5 ± 0.4 g cc^{-1}. A necessary condition for the formation of serpentine is a high flow rate of seawater into the upper mantle (Francis, 1981). High flow rates can be achieved through extensive faulting into the mantle and vigorous hydrothermal circulation. The Blanco Ridge exhibits vigorous seismicity with evidence of earthquakes (and thus faulting) to at least lower crust depths. It is likely that a large amount of fluid is able to flow along the transform fault of the Blanco Ridge which would allow the production of the low serpentine densities used in the model. Also, low crustal densities along the Blanco Ridge itself might be expected as a result of fracturing and brecciation of the crust by transform faulting. Abrams et al. (1988) modeled positive Bouguer anomalies along the Kane Fracture Zone and accounted for fault brecciation by assuming a 2 km thick, 1 km deep (beginning at the seafloor surface) low density zone ($\rho = 2.2$ g cm^3). To account for fault related brecciation along the BR, we included a region in the gravity model with the same size and density located along the inferred axis of the transform fault and above the serpentine-like low-density body.

The estimated 5 km width of the low density body is the approximate width of the Blanco Ridge and is consistent with the width of the fault zone inferred from surface exposures of faulting and fracturing ob-

served during the submersible dives. The 3 km thickness of the of the hypothesized low-density body is consistent with the thickness of serpentinized peridotite sections exposed at the Owens and Romanche Fracture Zones (Bonatti, 1978), although the 3 km is likely a minimum at these sites. The depth to the top of the low-density body along the BR is somewhat constrained by the thickness of the lower crustal rock sections exposed and sampled during the submersible dives. In each case, gabbro and basalt units with apparent thicknesses of up to 1 km were observed at outcrops along the Blanco Ridge. We infer then that a low-density body along the length of the BR probably has an average depth that is roughly the same as the thickness of lower crustal rocks exposed at the surface, or $\sim$1 km.

Discussion

Proposed transform ridge formation mechanisms

Transform parallel ridges are distinct morphologic features that have been observed along every major mid-ocean ridge system throughout the world. Previously proposed formation mechanisms for transform ridges include 1) serpentinite intrusion (Bonatti, 1976; Bonatti, 1978), 2) volcanism due to extension across the transform (Thompson and Melson, 1972), 3) dip-slip faulting from a component of extension or compression (Bonatti, 1978), or 4) uplift of the plate on the young side of the fracture zone due to thermal contrasts (Craig and MacKenzie, 1986). Serpentinite intrusion involves seawater percolating down along the fault to mantle depths where, once in the presence of water, mantle peridotite is altered to serpentinite. The serpentinite then rises diapirically and contributes to the formation of a transform parallel ridge (Bonatti, 1978). Ridge forming volcanic activity along fracture zones can occur due to hotspot volcanism. This has been observed at the Louisville Ridge/Heezen Fracture Zone (Epp, 1984), as ridge-perpendicular non-hotspot volcanoes near the East Pacific Rise (Batiza and Vanko, 1983), and as small linear chains of volcanoes along East Pacific Rise non-transform offsets (Lonsdale, 1985). Pockalny et al. (1995, 1996) demonstrated that a shift in the pole of plate rotation and a subsequent change in the ridge spreading direction has lead to extension and normal faulting along the Kane and Siqueiros Fracture Zones, and compression and reverse faulting along the 21°30′ N (Atlantic) and Clipperton Fracture Zones, with both faulting styles leading to the flexural formation of a transform parallel ridge. Hekinian et al. (1992) propose a combination of mechanisms for uplift of ultramafics and gabbros associated with the median ridge along the Garrett Transform. They suggest that the transform ridge formed through strike-slip (with a small component of dip-slip) tectonism, which allowed penetration of seawater to the lower crust upper mantle and enhanced serpentinization and diapiric ascent.

Blanco ridge stress state and crustal deformation

We suggest that compression did not play an important role in the formation of the Blanco Ridge. If uplift was due to underthrusting of the Juan de Fuca beneath the Pacific plate, then this would be manifested in earthquake focal mechanisms with predominantly reverse slip components. The acoustic locations, fault-parameter information, and slip vector estimates of 43 earthquakes ($M \geq 3.8$) that occurred along the eastern BTFZ from 1992–1997 reveal that the Blanco Ridge is a high-angle, right-lateral strike-slip fault with a small component of dip-slip where the Juan de Fuca plate is the hanging wall. The majority of the strike-slip mechanisms indicate the dip-slip component along the transform is typically normal motion. Assuming a 75 km displacement along the BR and a crustal thickness of 10 km, a small earthquake normal slip component ($\geq 8°$) similar to what is observed in the focal mechanism data would be a sufficient amount of dip-slip motion to expose lower oceanic crustal rocks. Furthermore, there is not a large age contrast between the two plates that could enhance underthrusting of the Pacific plate, with the Pacific being the same age or younger than the Juan de Fuca for all of the Blanco Ridge east of 128°20′ W.

In contrast, the clockwise change in Juan de Fuca plate motion that occurred 5 Ma (Wilson, 1993) would tend to cause oblique (NW–SE) compression along the eastern BTFZ. Evidence for the compressional/flexural origin of the Clipperton Transform Ridge exists in the morphologic similarity of the ridge and trough (that formed in the Cocos plate) to the flexure of an elastic plate with an endload, and the association of the ridge with Bouguer anomaly highs (Pockalny et al., 1997). It is possible that the Blanco Ridge was formed by uplift in part due to compression across the transform. Indeed, the free-air anomaly profile (upper right Figure 13) looks similar to a profile of the deflection of a plate (Pacific) under an end-

load. Three earthquakes (events 12, 22, and 35) show a slight reverse component, and it is possible that a component of compression across the eastern BTFZ is resulting in some underthrusting of the Pacific beneath the Juan de Fuca plate. However, the bulk of the fault parameter information indicates compression (thrust motion) is a minor factor in the formation of the BR.

Survey evidence for Blanco Ridge uplift

Brecciated and undeformed basalt, diabase, and gabbro samples were collected at the four submersible survey sites along the Blanco Ridge. Samples collected during the surveys suggest that the Blanco Ridge is comprised of an ocean crustal sequence that has been uplifted and highly fractured. The petrologic samples also appear to show an increase in elevation of the crustal section from east to west along the Blanco Ridge, with gabbros exposed at a shallower point farther west along the southern (Pacific plate side) of the Blanco Ridge flank. Further evidence for BR uplift can also be found in (1) the presence of sedimentary rocks found at the BR summit, (2) seismic reflection profiles across the BR showing uplift of turbidite sequences along the north and south ridge base, and (3) gravity and magnetic profiles that indicate possible basement uplift and a low-density zone centered on the ridge's Pacific plate side. The existence of a negative Bouguer anomaly over the BR suggests it is not an uncompensated stress-supported feature, but possibly compensated in an Airy fashion by an overthickened crust or a low density body. If the gravity data are correct and a low-density body is present in this tectonic environment, it would most likely be a serpentinized-peridotite diapir.

Blanco Ridge formation mechanism

The geology and geophysical data presented suggest several possibilities for Blanco Ridge formation. The formation mechanism preferred here is first, uplift achieved partially through strike-slip motion (with a small dip-slip component). Second, the strike-slip faulting may have allowed seawater penetration along the fault into the lower crust and upper mantle, which then enhanced formation and intrusion of a mantle-derived serpentinized-peridotite diapir into the shallow ocean crust causing further uplift along the fault. This is similar to a model proposed by Hekinian et al. (1992) for the Garret Transform along the East Pacific Rise. Formation of the diapir involves expansion of the mantle underlying the fracture zone by alteration of peridotite through deep hydrothermal circulation along the transform fault (Bonatti, 1976, 1978). Discrete diapirs along the transform fault might explain the morphology of the Blanco Ridge, which appears as a series of lozenge-shaped highs. Although no serpentinized-peridotite was found during these surveys (which may be a sample-density problem), it is a convenient mechanism to account for uplift within a narrow zone along a strike-slip fault where no ridge forming flexural features in the lithosphere are seismogenic.

A model for the composition, structure, and deformation of the Blanco Ridge is now proposed (Figure 14) based on the observations presented. The two cross-sections in Figure 14 are based on interpretation of the seafloor surveys done at sites 3 (Figure 14 right) and 4 (Figure 14 left), but also represent a synthesis of all data presented. A complete section (prior to the slump event) is hypothesized for the left cross section in Figure 14. The location of the active fault forming the transform plate boundary is constrained along the center of the Blanco Ridge by (1) the lineation at the ridge summit outlined in Figure 2, and (2) the mapping of faults and fissures and the ridge summit at sites 3 and 4. The transform fault may form the long, linear basin (notch) along the summit of the Blanco Ridge through brecciation of material along the fault and subsequent removal by ocean currents or mechanical weathering.

The Blanco Ridge shallows to the west, and based on the observations at sites 3 and 4, the deep ocean crustal rocks appear to shoal to the west as well (Figure 14). This may mean that a serpentinized-peridotite diapir, if it exists, also becomes progressively more shallow westward along the ridge. This may be a result of penetration of the serpentinized peridotite into the shallow portions of the crust, and/or the component of tectonic uplift. The result would be to force the deep oceanic-crustal rocks, at least on the Pacific plate side, closer to the seafloor surface before the ridge ends at the south end of Cascadia Depression. This is seemingly supported by the finding of diabase and basalt sections overlying a gabbro section in the Pacific crust at site 3 (Figure 11 and right-side Figure 14), while predominantly gabbros (and one basalt sample at the summit) were found along the south (Pacific) side of the ridge at site 4 (Figures 12 and left-side 14). The younger Juan de Fuca plate may have a full ocean crust section at these sites. In contrast, the cross section of Blanco Ridge crust at site 1 has basalt and diabase exposed along the scarp face, but no deeper crustal

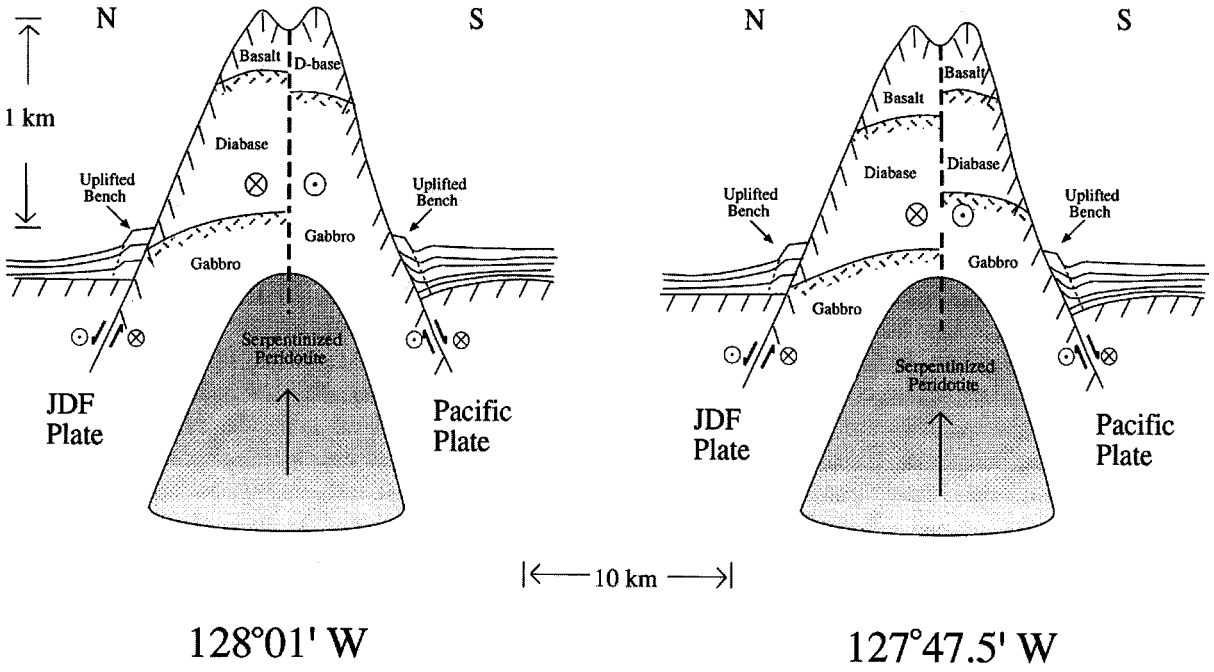

Figure 14. Proposed model for the composition, structure, and deformation history of the Blanco Ridge. Cross sections are meant to reflect interpretation of seafloor surveys from site 3 (right) and site 4 (left), but are a synthesis of all data presented here. The representation assumes an intact section of the Blanco Ridge for site 3 without the slump material removed. The less dense serpentinized-peridotite, formed through alteration of mantle material by deep hydrothermal circulation, causes uplift of ocean crust immediately adjacent to the active transform fault trace.

rocks. It could be that ridge uplift is reduced here since the normal faulting regime (and elevated crustal isotherms) of the Gorda Depression may inhibit the growth of a serpentinite diapir.

The observation of oblique compression along the eastern BTFZ (Figure 7, top) is not necessarily at odds with the Blanco Ridge model presented. Regional oblique compression is required to produce the observed strike-slip earthquakes, and could still allow for a small component of normal slip along the transform and an environment of diapiric uplift along the Blanco Ridge. Furthermore, the small and ephemeral nature of the focal mechanism dip-slip component suggests that the buoyancy effects due to a possible serpentinite intrusion are relatively equal on both the Juan de Fuca and Pacific plate sides of the transform, with the possibility that the Pacific plate side is slightly more buoyant as evidenced by the majority of mechanisms which indicate Juan de Fuca plate subsidence. But in general, the diapiric buoyancy effects may be offsetting any significant differential subsidence due to crustal age contrasts.

Secondary faulting and deformation along the Blanco Ridge

There appears to be two sets of ancillary faults that formed in response to transform motion, (1) the NE-SW trending abyssal ridges south of the Blanco Ridge, and (2) the NW-SE lineations along the base of the Blanco Ridge, just to the north and south of the ridge (L1 and L2 in Figure 1; white arrows in Figures 2 and 3). The NE–SW trending abyssal ridges south of the Blanco Ridge appear to bend more easterly near the transform fault. Thus they may be normal faults reactivated from relict spreading fabric within the Pacific plate. These proposed normal faults may be slipping in response to uplift along the Blanco Ridge, and forming drag folds in response to the strike-slip motion along the transform. The L1 and L2 lineations are interpreted here as surface expressions of dip-slip faults that may have formed at the toe of the turbidite sequences on the north and south sides of the BR. The lineations are represented as dashed lines at the base of the uplifted sediment benches in Figure 14. There is evidence of dip-slip motion along L1 where it is exposed at the slump scar at survey site 3. At this site, an ~200 m

ridge has formed along the lineation since it was exposed by the slump. Further evidence of uplift seems to exist in the bottom reflection profile in Figures 8a and 8b, where BR basement appears to be uplifted relative to the surrounding sediments. The L1 and L2 lineations/faults may have formed at the base of the turbidite sequences initially as diapiric normal faults in response to the Blanco Ridge serpentinite uplift, but because of regional right-lateral shear, they became elongate and exhibit predominantly strike-slip motion. Why these faults do not extend the full length of the BR is not known. At this point, more information is needed if the exact nature of the L1 and L2 features is to be better quantified.

The presence of mylonitized gabbro along the BTFZ (collected at the BR summit at site 2) provides evidence for shear deformation occurring to at least layer 3 depth above the Moho. Mylonites form due to extreme shear, at greenschist temperatures and pressures, under quasi-plastic flow in the crustal transition zone between brittle and plastic deformation (Sibson, 1986). In the case of oceanic crust, the brittle-plastic transition would be controlled by the depth of olivine plasticity (750–900 °C), and thus the brittle seismogenic layer might include the upper mantle (Yeats et al., 1997). This shear deformation hypothesis could not be tested, however, since no upper mantle samples were found.

Summary

The eastern BTFZ is a tectonic environment dominated by a right-lateral strike-slip fault experiencing a small component of uplift (possibly due to a serpentinite diapir) resulting in the formation of a transform-parallel ridge and the uplift of an oceanic crustal section. Formation mechanisms of the Blanco Ridge could be better constrained with drilling, deep-tow magnetics and gravity, and heat flow observations that would help further document the crustal composition, isotherm depth, *in situ* stress regimes, and coupling strength along the transform. The results of this study are summarized as follows:

(1) Acoustic locations, fault-parameter information, and slip vector estimates of 43 earthquakes ($M \geq 3.8$) that occurred along the eastern BTFZ over the last 5 years reveal that the Blanco Ridge is a high-angle right-lateral strike-slip fault, with a small component of dip-slip motion, where the Juan de Fuca plate is the hanging wall relative to the Pacific plate. Furthermore, the Cascadia and Gorda basins are undergoing normal faulting with extension predominantly oblique to the transform trend.

(2) Seafloor submersible observations agree with previous hypotheses that the active transform fault trace is the elongate narrow basin that runs the length of the BR summit.

(3) Petrologic samples indicate the Blanco Ridge is composed of an ocean crustal sequence that has been uplifted and highly fractured. The petrologic samples also appear to show an increase in elevation of the crustal section from east to west along the Blanco Ridge, with gabbros exposed at a shallower depth farther west along the southern (Pacific plate side) BR ridge flank.

(4) Supporting evidence for BR uplift exists in the seismic reflection profiles across the BR showing uplift of turbidite sequences along the north and south ridge base, and gravity and magnetics profiles that indicate possible basement uplift and a low-density zone centered on the ridge's Pacific plate side.

(5) The Blanco Ridge formation mechanism preferred here is first, uplift achieved partially through strike-slip motion with a small dip-slip component. Second, seawater penetration along the fault into the lower crust upper mantle, which then enhanced formation and intrusion of a mantle-derived serpentinized-peridotite diapir into the shallow ocean crust, causing further uplift along the fault.

Acknowledgments

The authors wish to thank Alice Davis and Jane Reid for the petrologic information, Vern Kulm for providing and discussing the 1969 Oregon State University seismic reflection data, Virginia Smith and Stephanie Ross for excellent at-sea support, and Matt Fowler and Paul Johnson for assistance with graphics. Also, the authors wish to thank the officers and crew of the R/V *Laney Chouest* and the U.S. Navy Deep Submergence Unit/Advanced Tethered Vehicle for expertise at sea without which this study could not have been conducted. This research was supported by the NOAA VENTS Program, PMEL contribution number 1974.

References

Abrams, L.J., Detrick, R.S. and Fox, P.J., 1988. Morphology and crustal structure of the Kane fracture zone transverse ridge, *J. Geophys. Res.* **93**: 3195–3210.

Aki, K. and Richards, P.G., 1980. *Quantitative Seismology, Theory and Methods*, W.H. Freeman and Company, New York.

Batiza, R. and Vanko, D., 1983. Volcanic development of small oceanic central volcanoes on the flanks of the East Pacific rise inferred from narrow beam echo sounder surveys, *Marine Geology* **54**: 53–90.

Bibee, L. D., 1986. Ocean Bottom Seismometer Measurements on the Gorda Ridge. *Open-File Report O-86-15*, State of Oregon Dept. of Geology and Mineral Industries, 25 pp.

Bergman, E.A. and Solomon, S.C., 1988. Transform fault earthquakes in the North Atlantic: source mechanism and depth of faulting, *J. Geophys. Res.* **93**: 9027–9057.

Bonatti, E., 1976. Serpentinite intrusions in the oceanic crust, *Earth Plan. Sci. Letts.*, **32**: 107–113.

Bonatti, E., 1978. Vertical tectonism in oceanic fracture zones, *Earth Planet. Sci. Lett.* **78**: 420–426.

Braunmiller, J., Leitner, B. and Nabelek, J., 1994. Monitoring Seismic Activity alongthe Blanco Fracture Zone with Regional Broad-Band Data, *Eos, Trans. Amer. Geophys. Union* **75**: 476.

Clague, D.A. and Holmes, M.L., 1987. Geology, petrology, and mineral potential of the Gorda Ridge, in Sholl, D.W., Grantz, A. and Vedder, J.G. (eds.), *Geology and Resource Potential of the Continental Margin of Western North America and Adjacent Ocean Basins - Beaufort Sea to Baja California*, Circum-PacificCouncil for Energy and Mineral Resources Earth Science Series Vol. 6: 563–580.

Craig, C.H. and MacKenzie, D., 1986. The Existence of a Thin, Low Viscosity Layer Beneath the Lithosphere. *Earth Planet Sci Lett.* **78**: 420–426.

deCharon, A.V., 1988. Structure and Tectonics of the Cascadia Segment, Central Blanco Transform Fault Zone, M.S. Thesis, Oregon State University, Corvallis, Oregon.

DeMets, C., Gordon, R.G., Argus, D.F. and Stein, S., 1990. Current plate motions, *Geophys. J. Int.* **101**: 425–478.

Dziak, R.P., Fox, C.G. and Embley, R.W., 1991. Relationship between the seismicity and geologic structure of the Blanco Transform Fault Zone, *Mar. Geophys. Res.* **13**: 203–208.

Dziak, R.P., Fox, C.G., Embley, R.W., Lupton, J.L., Johnson, G.C., Chadwick, W.W., Koski, R.A., 1996. Detection of and response to a probable volcanogenic T- wave event swarm on the western Blanco Transform Fault Zone, *Geophys. Res. Lett.* bf 23: 873–876.

Embley, R.W., 1985. A locally formed deep-ocean canyon system along the Blanco Transform, *Geo-Marine Lett.* **5**: 99–104.

Embley, R.W., Kulm, L.D., Massoth, G., Abbott, D. and Holmes, M., 1987. Morphology, structure, and resource potential of the Blanco Transform Fault Zone, In Sholl, D.W., Grantz, A. and Vedder, J.G., (eds.), *Geology and Resource Potential of the Continental Margin of Western North America and Adjacent Ocean Basins – Beaufort Sea to Baja California*, Circum-Pacific Council for Energy and Mineral Resources Earth Science Series, Vol. 6, pp. 549–562.

Embley R.W. and Wilson, D.S., 1992. Morphology of the Blanco Transform Fault Zone – NE Pacific: implications for its tectonic evolution. *Mar. Geophys. Res.* **14**: 25–45.

Epp, D., 1984. Possible perturbations to hotspot traces and implications for the origin and structure of the line islands, *J. Geophys. Res.* **89**: 11273–11286.

Fisk, M.R., Duncan, R.A., Fox, C.G. and Witter, J.B., 1993. Emergence and petrology of the Mendocino Ridge, *Mar. Geophys. Res.* **15**: 283–296.

Fox, C.G., Dziak, R.P., Matsumoto, H. and Schreiner, A.E., 1994. Potential for monitoring low-level seismicity on the Juan de Fuca Ridge using fixed hydrophone arrays, *Mar. Tech. Soc.* **27**: 22–30.

Francis, T.J.G., 1981. Serpentinization faults and their role in the tectonics of slow spreading ridges, *J. Geophys. Res.* **86**: 11616–11622.

Griggs, G.B. and Kulm, L.D., 1973. Origin and development of cascadia deep-sea channel, *J. Geophys. Res.* **9**: 6325–6339.

Hart, R., Pyle, D. and Robbins; J., 1990. Multistage hydrothermal systems in the Blanco Fracture Zone, In McMurray, G.R. (ed.), *Gorda Ridge, Seafloor Spreading Center in the United States' Exclusive Economic Zone*, Springer-Verlag, New York, pp. 51–76.

Hekinian, R., Bideau, D., Cannat, M., Francheteau, J. and Hebert, R., 1992. Volcanic activity and crust-mantle exposure in the ultrafast garret transform fault near 1328′ S in the Pacific, *Earth Planet Sci Lett.* **108**: 259–275.

Ibach, D.H. 1981. The Structure and Tectonics of the Blanco Fracture Zone. M.S.Thesis, Oregon State University, Corvallis, Oregon, 60 pp.

Ihmle, P.F. and Jordan, T.H., 1994. Teleseismic search for slow precursors to large earthqaukes, *Science* **266**: 1547–1551.

Kastens, K.A., MacDonald, K.C. and Becker, K., 1979. The Tamayo transfrom fault in the mouth of the Gulf of California, *Mar Geophys. Res.* **4**: 129–151.

Kastens, K.A., Ryan, W.B.F. and Fox, P.J., 1986. Structural and volcanic expression of a fast slipping ridge-transform-ridge plate boundary: sea Marc I and photographic surveys at the Clipperton transform fault, *J. Geophys. Res.* **91**: 3469–3488.

Koski, R.A., Embley, R.W., Ross, S.L., Dziak, R.P., Bohannon, R.G., Smith, V.K., Reid, J.A., Gray, L.B. and Tormanen, T.O., 1994. Tectonism and lithologic variation along the Blanco Ridge, Eastern Blanco Fracture Zone, NE Pacific: preliminary results from the PACNORWEST III cruise, *Eos, Trans. Amer. Geophys. Union* **75**: 656.

Lonsdale, P., 1985. Non-transform offsets of the Pacific-Cocos plate boundary and their traces on the rise flank, *Geo. Soc. Amer. Bull.* **96**: 313–329.

Macdonald, K.C., Fox, P.J., Alexander, R. T., Pockalny, R. and Gente, P., 1996. Volcanic growth faults and the origin of Pacific Abyssal Hills, *Nature* **380**: 125–129.

McDonald, M.A., Webb, S.C., Hildebrand, J.A. and Cornuelle, B.D., 1994. Seismic structure and anisotropy of the Juan de Fuca Ridge at 45° N, *J. Geophys. Res.* **99**: 4857–4873.

Mount, V.S. and Suppe, J., 1992. Present-day stress orientations adjacent to active strike-slip faults: California and Sumatra, *J. Geophys. Res.* **97**: 11995–12013.

Nabelek, J. and Xia, G., 1995. Regional and teleseismic analysis of the 29 March, 1993. Scotts Mills, Oregon, earthquake, *Geophys. Res. Lett.* **22**: 13–16.

National Earthquake Information Center, 1992. *Preliminary Determination ofEpicenters Catalog*, October.

Oppenheimer, D.H., Reasonberg, P.A. and Simpson, R.W., 1988. Fault plane solutions for the 1984 Morgan Hill, California earthquake sequence: evidence for the state of stress on the Calaveras Fault, *J. Geophys. Res.* **92**: 421–439.

Pockalny, R.A., Fox, P.J., Fornari, D.J., Macdonald, K.C. and Perfit, M.R., 1997. Tectonic reconstructions of the Clipperton and Siqueiros Fracture Zones: evidence and consequences of plate motion change for the last 3 Myr. *J. Geophys. Res.* **102**: 3167–3181.

Riddihough, R.P., Seemann, D.A. and Price, W.R., 1982. Juan de Fuca Plate Map: *JFP-8 Gravity Anomaly*. Earth Physics Branch: Department of Energy, Mines, and Resources, Ottawa, Canada.

Riddihough, R.P., 1984. Juan de Fuca Plate Map: *JFP-11 Magnetic Anomaly, Open File 85-20*. Pacific Geoscience Centre, Earth Physics Branch, Department of Energy, Mines, and Resources, Sidney, B.C. Canada.

Sibson, R.H., 1986. Earthquakes and rock deformation in Crustal Fault Zones, *Ann. Rev. Earth Planet. Sci.* **14**: 149–175.

Thompson, G. and Melson, W.G., 1972. The petrology of oceanic crust across fracture zones in the Atlantic Ocean: evidence for a new kind of seafloor spreading, *J. Geol.* **80**: 526–538.

Tobin, D.G. and Sykes, L.R., 1968. Seismicity and tectonics of the Norhteast Pacific Ocean, *J. Geophys. Res.* **94**: 3076–3089.

Wang, K., He, J. and Davis, E.E., 1997. Transform push, oblique subduction resistance, and intraplate stress of the Juan de Fuca Plate, *J. Geophys. Res.* **102**: 661–674.

Wilson, D.S., Hey, R.N. and Nishimura, C., 1984. Propagation as a mechanism of reorientation of the Juan de Fuca Ridge, *J. Geophys. Res.* **89**: 9215–9225.

Wilson, D.S., 1989. Deformation of the so-called Gorda Plate, *J. Geophys. Res.* **94**: 3065–3075.

Wilson, D.S., 1993. Confidence intervals for motion and deformation of the Juan de Fuca Plate, *J. Geophys. Res.* **98**: 16053–16071.

Yeats, R.S., Sieh, K. and Allen, C.R., 1997. *The Geology of Earthquakes*, Oxford University Press, 503 pp.